AIAA JOURNAL
Vol. 47, No. 9, September 2009

Modeling and Dynamics of Sandwich Beams with a Viscoelastic Soft Core

Ehab Hamed*
University of New South Wales, Sydney, New South Wales 2052, Australia
and
Oded Rabinovitch†
Technion—Israel Institute of Technology, 32000 Haifa, Israel

DOI: 10.2514/1.41840

The dynamic behavior of sandwich beams with a viscoelastic soft core is analytically studied. The analysis combines the concepts of viscoelasticity with those of the high-order sandwich beam theory and accounts for the shear and transverse (through the thickness) deformability and the viscoelastic effects through the constitutive laws of the core material. The beam model assumes no variation through the width. The viscoelastic response is introduced through the Kelvin–Voigt and Maxwell models, which characterize different materials and provide some of the fundamental building blocks for more refined viscoelastic theories. The governing equations that correspond to the two models and the solution procedures that combine time integration through Newmark's method with a numerical solution in space are derived. The formulation of a refined viscoelastic model based on the building blocks developed in the paper is analytically demonstrated. The capabilities of the model are studied numerically with emphasis on the time variation of the deflections and the interfacial shear and vertical normal stresses under step, impulse, and harmonic loads. A comparison between the theoretical results and experimental results available in the literature is also presented. The analytical models and the numerical study highlight some unique aspects of the dynamic response of sandwich beams with viscoelastic soft cores and provide fundamental analytical tools for their modeling.

Nomenclature

A^t_{xx}, A^b_{xx}	=	extensional rigidity of upper and lower sheets
a^σ_1, a^τ_1	=	viscous constants of the Kelvin–Voigt model
B^t_{xx}, B^b_{xx}	=	extensional-bending rigidity of upper and lower sheets
b	=	width of the beam
b^σ_1, b^τ_1	=	viscous constants of Maxwell's model
C_σ, C_w	=	unknown functions results from integration
D^t_{xx}, D^b_{xx}	=	flexural rigidity of upper and lower sheets
E_c	=	transverse modulus of elasticity of the core
G_c	=	shear modulus of the core
$g(x,t)$	=	typical unknown function
h_t, h_b, h_c	=	thicknesses of the upper sheet, lower sheet, and core layer
I_t, I_b	=	second moment of area of upper and lower sheets
L	=	length of the beam
$\bar{M}_{jt}, \bar{M}_{jb}$	=	concentrated bending moments at the upper and lower sheets
M^t_{xx}, M^b_{xx}	=	bending moment stress resultant in the upper and lower sheets
m_t, m_b, m_c	=	mass per unit length of upper sheet, lower sheet, and core layer
m_{xt}, m_{xb}	=	distributed bending moments at the upper and lower sheets
$\bar{N}_{jt}, \bar{N}_{jb}$	=	concentrated axial loads at the upper and lower sheets
N^t_{xx}, N^b_{xx}	=	in-plane stress resultant in the upper and lower sheets
n_{xt}, n_{xb}	=	distributed axial loads at the upper and lower sheets
$\bar{P}_{jt}, \bar{P}_{jb}$	=	concentrated vertical loads at the upper and lower sheets
q_{zt}, q_{zb}	=	distributed vertical loads at the upper and lower sheets
s^n_m	=	initial conditions at each region used in the multiple shooting method
u_{ot}, u_{ob}	=	longitudinal deformation at the reference line of upper and lower sheets
u_t, u_b, u_c	=	longitudinal deformation of upper sheet, lower sheet, and core layer
V_t, V_b, V_c	=	volume of upper sheet, lower sheet, and core layer
w_t, w_b, w_c	=	transverse deflection of upper sheet, lower sheet, and core layer
z_c	=	local coordinate from the upper core-face interface downward
z_t, z_b	=	local coordinates from the midheight of the face sheets downward
β, γ	=	parameters for Newmark's time integration
γ^c_{xz}	=	shear angle in the core
Δt	=	time step interval
δ_D	=	Dirac function
δK	=	virtual work of the inertial forces
$\delta' U$	=	virtual work of the internal stresses
δW	=	virtual work of the external loads
ε^c_{zz}	=	transverse normal strain in the core
$\varepsilon^t_{xx}, \varepsilon^b_{xx}$	=	longitudinal strains in the upper and lower face sheets
η_τ, η_σ	=	material loss factor in shear and the transverse direction
λ, κ	=	indicators for the boundary conditions
ρ_t, ρ_b, ρ_c	=	mass density of the upper sheet, lower sheet, and core layer

Received 28 October 2008; revision received 26 January 2009; accepted for publication 28 April 2009.

*Research Associate, Center for Infrastructure Engineering and Safety, School of Civil and Environmental Engineering; e.hamed@unsw.edu.au (Corresponding Author).

†Associate Professor and Horev Fellow, Supported by the Taub Foundation, Faculty of Civil and Environmental Engineering. AIAA Member.

σ_{xx}^t, σ_{xx}^b = longitudinal stresses in the upper and lower face sheets
σ_{zz}^c = transverse normal stresses in the core
τ_{xz}^c = shear stress in the core

I. Introduction

THE use of sandwich beams made of thin and stiff face sheets connected by a thick and compliant (soft) core is widely used in aerospace constructions as well as in many other structural applications. The vibration of these structures is one of their basic design aspects, where the minimization of the vibration amplitudes is commonly required to mitigate fatigue failures. The dynamic behavior of the sandwich structure is commonly enhanced through the use of thick, shear deformable and transversely (through the thickness) compressible, viscoelastic core materials along with stiff and thin sheets. In this configuration, the overall flexural rigidity of the beam remains high enough to resist the imposed loads, while the viscoelastic layer provides the structure with damping characteristics and a "passive damping treatment" [1–5]. During vibrations, the viscoelastic core deforms in transverse shear and in the transverse (through the thickness) direction through interaction with the adjacent stiff face sheets, and the resulting energy stored in the viscoelastic core is partially dissipated to the surrounding medium. This behavior contributes to the multifunctionality of the sandwich structural system that combines load resistance with effective damping and energy dissipation.

The viscoelastic features are effective and attractive for enhancing the damping characteristics of sandwich beams. To take advantage of that, a thorough understanding of their impact on the dynamic behavior of sandwich structures is required. Among the critical physical aspects that make the analysis of the dynamic behavior of sandwich structures with viscoelastic soft cores a challenging and complicated task are the deformability of the core in shear and in the transverse direction and the interaction between the transverse shear and the transverse normal stresses, mainly near edges, irregular points, or concentrated loads [6,7]. These stresses play a critical role in the localized and global response of the sandwich structure, and, in many cases, govern its failure mechanism. The viscoelastic characteristics of the core material may modify the distributions and the magnitudes of these stresses, as well as those of the deflections and stress resultants. This aspect and the influence of the viscoelastic nature of the core on the overall and localized dynamic behavior of the sandwich beam are studied here.

Along with the aforementioned, other aspects of the viscoelastic response also contribute to the complexity of the problem. Among these, the frequency, temperature, and rate dependency of the properties of the core material [8–10], the coupling of the vibration modes [11], the influence of the core damping characteristics (material loss factor) on the overall damping of the sandwich beam, the effect of the geometrical and mechanical properties of the sandwich layers on the overall damping characteristics [12], and the potential nonlinear material behavior of the viscoelastic core at high frequency loading [13] can be listed.

Many efforts were made to study the vibration response of sandwich beams with viscoelastic cores. Kerwin [14] analyzed a simply supported sandwich beam using a complex shear modulus for the representation of the viscoelastic core. DiTaranto [15] derived a sixth-order differential equation of motion in terms of the longitudinal displacements to study the viscoelastic response of sandwich beams based on the complex shear modulus. Mead and Markus [11] studied the forced vibration response of sandwich beams with different boundary conditions by using the complex shear modulus approach and the assumption of linear distribution of the longitudinal displacement in the core. Following [11], many research works studied the viscoelastic response of sandwich beams. Rao [12] derived a set of equations of motion for sandwich beams using energy approaches. Lifshitz and Liebowitz [1] developed an automated optimization numerical program for designing three-layer sandwich beams for maximum damping. Galucio et al. [16] used the finite element formulation assuming Euler–Bernoulli's hypotheses for the elastic faces and Timoshenko's ones for the viscoelastic core. Sakiyama et al. [17], Meunier and Shenoi [18], and Hunston et al. [19] investigated the free and forced vibration response of sandwich beams assuming that the core layer is stiff in the transverse (height) direction and deforms in pure shear only. Pradeep et al. [20] assumed that the dissipation in the core is only due to shear, and Nayfeh [21] adopted the lumped mass and stiffness approach to study the flexural vibration response of viscoelastic sandwich beams but without the consideration of local effects at the edges or near concentrated loads.

The aforementioned studies, as well as many others, designate three main aspects that require further investigation:

1) The studies focused on the influence of the viscoelasticity of the core material on the overall harmonic response of the sandwich beam without considering its influence on the local shear and normal transverse stresses in the core. In general, the behavior of sandwich beams is characterized by many local effects that govern their delamination and debonding failures [22]. The effect of the viscoelastic nature of the core on these local effects should be clarified.

2) The preceding theoretical models assumed that the height of the core remains unchanged, that is, incompressible, and that the damping in the core is mainly due to shear deformations. Modern sandwich beams are, however, made of compressible foam core materials that are usually associated with localized displacements through the height of the core and with different transverse normal stresses at the interfaces. As a consequence, the transverse (through the height) damping can play an important role in the dynamic response of the sandwich beam and should therefore be considered [7,23].

3) The aforementioned studies used the complex shear modulus approach to model the viscoelastic characteristics of the core. This approach can be used for harmonic oscillations but it does not address the transient response of the structure, which could be of concern in many practical cases [3,24].

To overcome the limitations of the complex modulus approach, Wang and Wereley [3] developed a spectral finite element model in the frequency domain for the dynamic analysis of sandwich beams. However, the transverse flexibility through the height and the transverse damping of the core layer were not considered. Douglas and Yang [23] presented a theoretical model that accounts for the transverse flexibility and damping of the viscoelastic core. The model focused only on the transverse behavior of the structure by modeling the core layer as a transverse spring with a complex constant. The shear deformations of the core, the interaction of the shear and transverse normal stresses, and the variation of stresses through the height of the core were not considered. However, the simpler model of [23] showed very good agreement with the experiment with thick cores, and provided some important guidance as to the conditions under which the dissipation from transverse stretching is significant, such as cases that included delamination or debonding. Also Douglas [25], who extended the theoretical model of [23] to include rotary inertia and shear deformation in the elastic layers, compared the response of transverse stretching alone with that for shear alone. A model that accounts for the transverse damping only but considers the inertial forces of the core layer was presented by Sisemore and Darvennes [7]. Bai and Sun [26] used a high-order theory that accounts for the deformability of the core in shear and in the transverse direction. Yet, the influence of the viscoelastic behavior of the core in the transverse direction was ignored. In addition, the model was limited to the response of sandwich panels under forced harmonic loads. Baber et al. [27] developed a finite element model for harmonically excited viscoelastic sandwich beams based on the theoretical approach of [26]. Based on the complex modulus approach, Miles and Reinhall [28] developed a theoretical model that accounts for dissipation through both shear and transverse normal stresses in the viscoelastic layer. The model assumed a constant transverse normal strain and a linear variation of the shear angle through the thickness of the core. These two assumptions are not compatible in terms of material point (continuum) level equilibrium in the core, they lead to constant transverse normal stresses through the thickness of the core, and they violate the shear stress free boundary condition at the free faces of the core. Based on [6,22,29–32], the transverse normal stresses vary through the height of the core, attain different

values and different distributions at the upper and the lower interfaces, and, in many cases, even have different signs (tension/compression) at the different interfaces. These effects must be considered in the dynamic analysis of the viscoelastic sandwich beam. Furthermore, to quantify the transverse stress concentrations at the ends of the core, which are critical for the design of sandwich beams, the shear stress free boundary condition and the interaction between the shear stresses and the transverse normal stresses stemming from the continuum level equilibrium conditions must be fulfilled. In addition, Miles and Reinhall [28] focused only on the determination of the modal loss factors and frequencies of sandwich beams with a relatively thin viscoelastic layer by a free vibration analysis using the Ritz method with assumed displacement fields through the length of the beam. Thus, the behavior of sandwich beams with a thick core under different types of dynamic loads, in which the aforementioned effects are even more pronounced, was not studied.

A high-order dynamic theory that accounts for the shear and transverse deformability of the core was presented by Frostig and Baruch [6], Frostig and Thomsen [29], and Schwarts-Givli et al. [30–32]. These works did not take the viscoelastic features of the core or the damping effects in the sandwich structure into account. The damping and viscoelastic dynamic response of reinforced concrete flexural members strengthened with adhesively bonded composite materials were studied by Hamed and Rabinovitch [33]. The model used a high-order theory [22], but it was limited to the Kelvin–Voigt model of viscoelasticity [34] and did not address the unique aspects of the sandwich structure. A preliminary Kelvin–Voigt model for sandwich beams was also presented by Hamed and Rabinovitch [35]. Yet, due to the limitation to only one phase of the viscoelastic phenomena reflected by the Kelvin–Voigt model, this model could not be used for the description of the entire spectrum of the viscoelastic response.

The objective of this paper is to analytically study and describe the localized and overall damped dynamic behavior of modern sandwich beams with a shear deformable and transversely compressible viscoelastic core. For that purpose, a theoretical model for the dynamic analysis of a sandwich beam made of a viscoelastic soft core and elastic composite laminated face sheets is developed. The theoretical approach combines the basic concepts of the high-order sandwich theory [6,22] with the Kelvin–Voigt and Maxwell models of viscoelasticity. The four basic building blocks for linear viscoelasticity are the elastic solid (single spring), viscous fluid (single dashpot), Kelvin–Voigt solid (spring and dashpot in parallel), and Maxwell fluid (spring and dashpot in series). The investigation of the latter two models, along with the elastic solid one, which is included in the numerical study and can be degenerated from the current formulation to provide the one given in [6] as a particular case, provide a theoretical basis for other, more complex, and more refined viscoelastic theories, such as the standard linear solid model (Maxwell's model in parallel with an elastic solid), the generalized Maxwell model, or others [8,34]. The model developed here accounts for the high-order deformation fields and for the viscoelastic effect in transverse shear and in the transverse normal direction in the core under transient and steady-state dynamic response. On the other hand, following Frostig and Baruch [6], the high-order velocity and acceleration effects are not accounted for.

The theoretical formulation uses dynamic equilibrium, compatibility requirements between the structural components, and the viscoelastic models. The principle of virtual work is used for the derivation of the equations of motion. The lamination theory is used for the modeling of the elastic composite laminated face sheets. To account for the response of the structure under different dynamic loads (not necessarily harmonic ones), the fundamental forms of the Kelvin–Voigt and Maxwell models [34] are implemented in the constitutive relations of the core. The two types of viscoelastic models account for the energy dissipation. The temperature rise in the core due to dissipation of energy is, however, neglected, and it is assumed that the viscoelastic constants of the core material are independent of the temperature and the frequency [8,16]. Following Frostig et al. [6,22], the longitudinal stiffness of the core is neglected with respect to that of the face sheets. It is also assumed that the loads are exerted at the face sheets and that the stress and deformation fields are uniform through the width. Finally, as a first step, the analysis is conducted in the framework of linear elasticity, linear viscoelasticity, and geometrical linearity (small deflections).

II. Mathematical Formulation

The mathematical formulation includes the derivation of the equations of motion and the initial and boundary conditions. The viscoelastic characteristics of the core material are then introduced through the constitutive relations, and the governing equations that correspond to the Kelvin–Voigt and Maxwell models for the core material are derived. The sign conventions for the coordinates, displacements, loads, stresses, and stress resultants appear in Fig. 1.

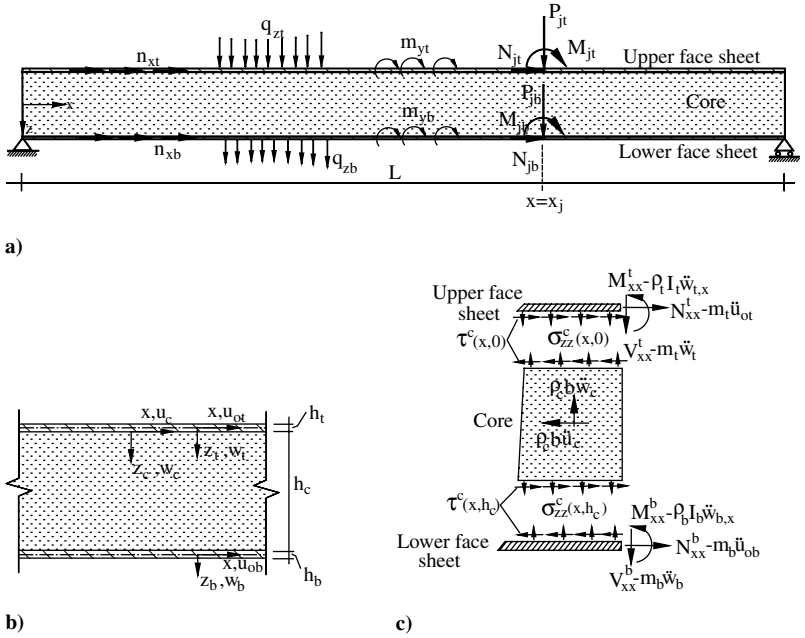

Fig. 1 Geometry, loads, sign conventions, and stress resultants: a) geometry and loads, b) deformations and coordinate system, c) stresses and stress resultant.

The principle of virtual work requires

$$\delta K + \delta' U + \delta W = 0 \tag{1}$$

where δK is the virtual work of the inertial forces, $\delta' U$ is the virtual work of the stresses, δW is the virtual work of the external loads, and the prime designates that U is not necessarily a potential function. The virtual work of the inertial forces is

$$\begin{aligned}\delta K = -\Bigg[&\int_{V_t} \rho_t[\ddot{w}_t(x,z_t,t)\delta w_t(x,z_t,t) + \ddot{u}_t(x,z_t,t)\delta u_t(x,z_t,t)]\,\mathrm{d}V_t \\ &+ \int_{V_b} \rho_b[\ddot{w}_b(x,z_b,t)\delta w_b(x,z_b,t) + \ddot{u}_b(x,z_b,t)\delta u_b(x,z_b,t)]\,\mathrm{d}V_b \\ &+ \int_{V_c} \rho_c[\ddot{w}_c(x,z_c,t)\delta w_c(x,z_c,t) + \ddot{u}_c(x,z_c,t)\delta u_c(x,z_c,t)]\,\mathrm{d}V_c\Bigg]\end{aligned} \tag{2}$$

where t, b, and c refer to the upper face sheet, the lower face sheet, and the core, respectively, ρ_i is the mass density of the upper ($i = t$) and the lower ($i = b$) face sheets and the core ($i = c$), $w_i(x, z_i, t)$, and $u_i(x, z_i, t)$ are the transverse and longitudinal displacements of each component, respectively, V_i ($i = t,\ b,\ c$) is the volume of each component, and $\dot{()}$ denotes a derivative with respect to time. The virtual work of the stresses [36] is

$$\begin{aligned}\delta' U = -\Bigg[&\int_{V_t} \sigma^t_{xx}(x,z_t,t)\delta\varepsilon^t_{xx}(x,z_t,t)\,\mathrm{d}V_t \\ &+ \int_{V_b} \sigma^b_{xx}(x,z_b,t)\delta\varepsilon^b_{xx}(x,z_b,t)\,\mathrm{d}V_b \\ &+ \int_{V_c} [\tau^c_{xz}(x,z_c,t)\delta\gamma^c_{xz}(x,z_c,t) + \sigma^c_{zz}(x,z_c,t)\delta\varepsilon^c_{zz}(x,z_c,t)]\,\mathrm{d}V_c\Bigg]\end{aligned} \tag{3}$$

where σ^i_{xx} and ε^i_{xx} ($i = t,\ b$) are the longitudinal stresses and strains, respectively, in the upper and the lower face sheets, τ^c_{xz} and σ^c_{zz} are the transverse shear and transverse normal stresses in the core, respectively, and γ^c_{xz} and ε^c_{zz} are the transverse shear angle and transverse normal strain in the core, respectively.

The kinematic relations of the face sheets assume small displacements and negligible shear deformations and follow the Bernoulli–Euler theory:

$$w_i(x, z_i, t) = w_i(x, t) \tag{4a}$$

$$u_i(x, z_i, t) = u_{oi}(x, t) - z_i w_{i,x}(x, t) \tag{4b}$$

$$\varepsilon^i_{xx}(x, z_i, t) = u_{oi,x}(x, t) - z_i w_{i,xx}(x, t) \tag{4c}$$

where z_t and z_b are measured from the midheight of the face sheets downward, u_{oi} is the longitudinal deformation at the reference line (midheight) of the face sheets (see Fig. 1), and $()_{,x}$ is a derivative with respect to x.

The kinematic relations for the core are

$$\varepsilon^c_{zz}(x, z_c, t) = w_{c,z}(x, z_c, t) \tag{5a}$$

$$\gamma^c_{xz}(x, z_c, t) = u_{c,z}(x, z_c, t) + w_{c,x}(x, z_c, t) \tag{5b}$$

The virtual work of the external loads equals

$$\begin{aligned}\delta W = &\int_{x=0}^{x=L} [q_{zi}(x,t)\delta w_i(x,t) + n_{xi}(x,t)\delta u_{oi}(x,t) \\ &+ m_{yi}(x,t)\delta w_{i,x}(x,t)]\,\mathrm{d}x \\ &+ \sum_{j=1}^{\mathrm{NC}} \int_{x=0}^{x=L} [\bar{P}_{ji}(t)\delta w_i(x_j,t) + \bar{N}_{ji}(t)\delta u_{oi}(x_j,t) \\ &+ \bar{M}_{ji}(t)\delta w_{i,x}(x_j,t)]\delta_D(x-x_j)\,\mathrm{d}x \quad (i = t, b)\end{aligned} \tag{6}$$

where $q_{zi}(x, t)$, $n_{xi}(x, t)$, $m_{yi}(x, t)$ are the time-dependent external distributed loads and bending moments exerted at the upper ($i = t$) and the lower ($i = b$) face sheets, respectively, $\bar{P}_{ji}(t)$, $\bar{N}_{ji}(t)$, and $\bar{M}_{ji}(t)$ are the dynamic concentrated loads and bending moments at $x = x_j$, δ_D is the Dirac function, NC is the number of concentrated loads, and L is the length of the beam.

The assumption of perfect bonding between the components is introduced through compatibility requirements imposed on the transverse and the longitudinal deformations at the interfaces of the core:

$$w_c(x, z_c = 0, t) = w_t(x, t) \tag{7a}$$

$$u_c(x, z_c = 0, t) = u_{ot}(x, t) - \frac{h_t}{2} w_{t,x}(x, t) \tag{7b}$$

$$w_c(x, z_c = h_c, t) = w_b(x, t) \tag{8a}$$

$$u_c(x, z_c = h_c, t) = u_{ob}(x, t) + \frac{h_b}{2} w_{b,x}(x, t) \tag{8b}$$

where h_c, h_t, and h_b are the thicknesses of the core, the upper and lower face sheets, respectively, and z_c is measured from the upper core-face interface (Fig. 1a).

Although the high-order terms of the displacements in the transverse direction are considered, following Frostig and Baruch [6] and the findings of Sokolinsky and Nutt [37], who have made an attempt to consider the high-order velocity and acceleration fields of the core through its thickness and compared the results with [6], the distributions of the velocities and accelerations are assumed linear through the height of the core. For example, the velocities are

$$\dot{w}_c(x, z_c, t) = [\dot{w}_b(x, t) - \dot{w}_t(x, t)]\frac{z_c}{h_c} + \dot{w}_t(x, t) \tag{9}$$

$$\begin{aligned}\dot{u}_c(x, z_c, t) = \Bigg(&\dot{u}_{ob}(x, t) + \frac{h_b}{2}\dot{w}_{b,x}(x, t) - \dot{u}_{ot}(x, t) \\ &+ \frac{h_t}{2}\dot{w}_{t,x}(x, t)\Bigg)\frac{z_c}{h_c} + \dot{u}_{ot}(x, t) - \frac{h_t}{2}\dot{w}_{t,x}(x, t)\end{aligned} \tag{10}$$

As the motivation of this paper is to investigate the effect of the viscoelasticity of the core material rather than the influence of higher-order distributions of the velocity and acceleration fields, the reader is referred to [31,32] for a different approach that can incorporate the higher-order inertia effects.

Using the variational principle [Eqs. (1–3) and (6)], along with the kinematic relations [Eqs. (4) and (5)], the compatibility conditions [Eqs. (7) and (8)], and the velocity and acceleration fields of the core [Eqs. (9) and (10)], the equations of motion read (also see [6,33,35])

$$\begin{aligned}&N^t_{xx,x}(x,t) + b\tau^c_{xz}(x, z_c = 0, t) - m_t\ddot{u}_{ot}(x,t) + \frac{m_c h_t}{6}\ddot{w}_{t,x}(x,t) \\ &\quad - \frac{m_c h_b}{12}\ddot{w}_{b,x}(x,t) - \frac{m_c}{3}\ddot{u}_{ot}(x,t) - \frac{m_c}{6}\ddot{u}_{ob}(x,t) + n_{xt}(x,t) = 0\end{aligned} \tag{11}$$

$$\begin{aligned}&N^b_{xx,x}(x,t) - b\tau^c_{xz}(x, z_c = h_c, t) - m_b\ddot{u}_{ob}(x,t) + \frac{m_t h_t}{12}\ddot{w}_{t,x}(x,t) \\ &\quad - \frac{m_c h_b}{6}\ddot{w}_{b,x}(x,t) - \frac{m_c}{6}\ddot{u}_{ot}(x,t) - \frac{m_c}{3}\ddot{u}_{ob}(x,t) + n_{xb}(x,t) = 0\end{aligned} \tag{12}$$

$$M^t_{xx,xx}(x,t) + b\frac{h_t}{2}\tau^c_{xz,x}(x,z_c=0,t) + b\sigma^c_{zz}(x,z_c=0,t) - m_t\ddot{w}_t(x,t) + \rho_t I_t\ddot{w}_{t,xx}(x,t) - \frac{m_c h_t}{12}\left(\frac{2\ddot{w}_b(x,t)+4\ddot{w}_t(x,t)}{h_t} - h_t\ddot{w}_{t,xx}(x,t) + \frac{h_b}{2}\ddot{w}_{b,xx}(x,t) + 2\ddot{u}_{ot,x}(x,t) + \ddot{u}_{ob,x}(x,t)\right) + q_{zt}(x,t) - m_{yt,x}(x,t) = 0 \quad (13)$$

$$M^b_{xx,xx}(x,t) + b\frac{h_b}{2}\tau^c_{xz,x}(x,z_c=h_c,t) - b\sigma^c_{zz}(x,z_c=h_c,t) - m_b\ddot{w}_b(x,t) + \rho_b I_b\ddot{w}_{b,xx}(x,t) - \frac{m_c h_b}{12}\left(\frac{2\ddot{w}_t(x,t)+4\ddot{w}_b(x,t)}{h_b} + \frac{h_t}{2}\ddot{w}_{t,xx}(x,t) - h_b\ddot{w}_{b,xx}(x,t) - 2\ddot{u}_{ob,x}(x,t) - \ddot{u}_{ot,x}(x,t)\right) + q_{zb}(x,t) - m_{yb,x}(x,t) = 0 \quad (14)$$

$$\tau^c_{xz,x}(x,z_c,t) + \sigma^c_{zz,z}(x,z_c,t) = 0 \quad (15)$$

$$\tau^c_{xz,z}(x,z_c,t) = 0 \quad (16)$$

where m_i ($i = t, b, c$) is the mass per unit length of the upper face sheet, the lower face sheet, and the core layer, respectively, N^i_{xx}, M^i_{xx} ($i = t, b$) are the in-plane and bending moment stress resultant in the face sheets, b is the width of the beam, and I_i ($i = t, b$) is the second moment of area of each face sheet. Note that the mathematical model presented in [6], which focused on the free vibration behavior of elastic sandwich beams only, does not account for a complete dynamic analysis under different loads, neither for the effect of the rotary inertia of the face sheets nor the viscoelastic effects studied in this paper. The free vibration equation presented in [6] can be degenerated from Eqs. (11–16) by dropping the external forces and the rotary inertia terms of the face sheets.

The viscoelastic characteristics of the core layer are introduced through the constitutive relations. The formulation follows the main steps developed in [6,22]; yet they are modified and generalized to account for the viscoelasticity of the core. A variety of models were proposed in the literature for the modeling of different viscoelastic materials. Most of these models are, however, based on the fundamental Kelvin–Voigt and Maxwell models [8,34] (as well as the purely elastic case and the purely viscous case). The Kelvin–Voigt and Maxwell models, which can represent different core materials and different aspects of the viscoelastic dynamic response, are studied here (the elastic case, which is addressed in [6] is considered by degenerating the viscoelastic models studied here). Although the core never actually behaves like Maxwell's model nor like a Kelvin–Voigt model with a single retardation time, but according to advanced combinations of viscoelastic models, it is of significant impact to show how the structure behaves according to these two models when used separately.

In all cases, the discussion limits the viscoelastic effects to the core material only and the constitutive relations of the face sheets assume a linear elastic behavior. Thus, the constitutive laws for the laminated face sheets are

$$N^i_{xx}(x,t) = b[A^i_{xx}u_{oi,x}(x,t) - B^i_{xx}w_{i,xx}(x,t)] \quad (17)$$

$$M^i_{xx}(x,t) = b[B^i_{xx}u_{oi,x}(x,t) - D^i_{xx}w_{i,xx}(x,t)] \quad (18)$$

where A^i_{xx}, B^i_{xx}, and D^i_{xx} are the extensional, extensional-bending, and flexural rigidities of the face sheets in the x direction.

A. Kelvin–Voigt Model

The formulation of the Kelvin–Voigt model follows [33,35].

1. Constitutive Relations

According to the Kelvin–Voigt model with a single retardation time, the constitutive relations of the viscoelastic core are

$$\sigma^c_{zz}(x,z_c,t) = E_c\varepsilon^c_{zz}(x,z_c,t) + a^\sigma_1 E_c\dot{\varepsilon}^c_{zz}(x,z_c,t) \quad (19)$$

$$\tau^c_{xz}(x,z_c,t) = G_c\gamma^c_{xz}(x,z_c,t) + a^\tau_1 G_c\dot{\gamma}^c_{xz}(x,z_c,t) \quad (20)$$

where E_c and G_c are the transverse modulus of elasticity and shear modulus of the core, respectively, $\dot{\varepsilon}^c_{zz}$ and $\dot{\gamma}^c_{xz}$ are the transverse normal strain rate and the shear angle rate, respectively, and a^σ_1 and a^τ_1 are the viscous constants of the Kelvin–Voigt model. In the general case, the elastic properties and the viscous constants depend on the frequency and temperature. These effects are not studied here and the values of the viscous constants are determined based on a characteristic range of undamped frequencies and maintained constant during the dynamic time domain analysis [8]. In addition, the modeling assumes a constant and prescribed temperature and neglects the temperature rise due to the energy dissipation.

2. Stress and Displacement Fields

Equations (15) and (16) yield the following stress fields (also see [6,22,33,35]):

$$\tau^c_{xz}(x,z_c,t) = \tau^c_{xz}(x,t) = \tau^c(x,t) \quad (21)$$

$$\sigma^c_{zz}(x,z_c,t) = -\tau^c_{,x}(x,t)z_c + C_\sigma(x,t) \quad (22)$$

where $C_\sigma(x,t)$ is a function of x and t only.

The transverse displacement is determined using the kinematic and the constitutive relations [Eqs. (5a) and (19)] and integration through the height of the core:

$$[w_c(x,z_c,t) + a^\sigma_1\dot{w}_c(x,z_c,t)] = \frac{[(-\tau^c_{,x}(x,t)z_c^2/2) + C_\sigma(x,t)z_c]}{E_c} + C_w(x,t) \quad (23)$$

where $C_w(x,t)$ is a second function of x and t only. Using the transverse velocity field of the core [Eq. (9)], the transverse displacement field takes the following form:

$$w_c(x,z_c,t) = -a^\sigma_1\left(\frac{z_c}{c_c}\dot{w}_b(x,t) + \left(1-\frac{z_c}{c_c}\right)\dot{w}_t(x,t)\right) - \frac{z_c^2}{2E_c}\tau^c_{,x}(x,t) + \frac{z_c}{E_c}C_\sigma(x,t) + C_w(x,t) \quad (24)$$

$C_\sigma(x,t)$ and $C_w(x,t)$ are determined using the compatibility conditions of the transverse displacement at the core-sheet interfaces [Eqs. (7a) and (8a)] and, following [33,35], the transverse displacement and normal stresses through the height of the core become

$$w_c(x,z_c,t) = -\tau^c_{,x}(x,t)\frac{(z_c^2 - h_c z_c)}{2E_c} + \frac{[w_b(x,t) - w_t(x,t)]z_c}{h_c} + w_t(x,t) \quad (25)$$

$$\sigma^c_{zz}(x,z_c,t) = \frac{E_c\left\{w_b(x,t) - w_t(x,t) + a^\sigma_1[\dot{w}_b(x,t) - \dot{w}_t(x,t)]\right\}}{h_c} - \tau^c_{,x}(x,t)\frac{(2z_c - h_c)}{2} \quad (26)$$

The distribution of the longitudinal displacement is determined using the kinematic relation [Eq. (5b)] and the constitutive relations [Eq. (20)]. Integration through the height of the core yields

$$[u_c(x,z_c,t)+a_1^\tau \dot{u}_c(x,z_c,t)] = \int \frac{\tau^c(x,t)}{G_c}\,\mathrm{d}z_c - \int [w_{c,x}(x,z_c,t) + a_1^\tau \dot{w}_{c,x}(x,z_c,t)]\,\mathrm{d}z_c + C_u(x,t) \tag{27}$$

where $C_u(x,t)$ is determined through the compatibility condition of the longitudinal displacement at the upper interface [Eq. (7b)]. Explicitly, u_c is determined by introducing the velocity fields [Eq. (9) and (10)] and the transverse displacement field [Eq. (25)] into Eq. (27) (also see [33,35]):

$$\begin{aligned} u_c(x,z_c,t) &= \frac{\tau^c(x,t)z_c}{G_c} + \frac{\tau^c_{,xx}(x,t)}{2E_c}\left(\frac{z_c^3}{3} - h_c\frac{z_c^2}{2}\right) \\ &- \frac{w_{b,x}(x,t)z_c^2}{2h_c} - w_{t,x}(x,t)\left(-\frac{z_c^2}{2h_c} + z_c + \frac{h_t}{2}\right) + u_{ot}(x,t) \\ &- a_1^\tau\left(\frac{z_c h_b}{2h_c} + \frac{z_c^2}{2h_c}\right)\dot{w}_{b,x}(x,t) - a_1^\tau\left(z_c - \frac{z_c^2}{2h_c} + \frac{z_c h_t}{2h_c}\right)\dot{w}_{t,x}(x,t) \\ &+ a_1^\tau \frac{z_c}{h_c}[\dot{u}_{ot}(x,t) - \dot{u}_{ob}(x,t)] \end{aligned} \tag{28}$$

By comparing the stress and displacement fields obtained here for the core layer with the ones presented in [6,22], it can be seen that the transverse displacement field is identical to the one presented in [6,22], whereas the viscoelasticity of the core introduces additional viscous terms to the fields of the transverse stresses and the longitudinal deformations. Setting the viscous coefficients a_1^τ and a_1^σ to zero, reduces Eqs. (25), (26), and (28) to the elastic case and recovers the stress and displacement fields presented in [6,22]. Also note that, as opposed to Miles and Reinhall [28], which assumed a constant transverse normal strain and a linear variation of the shear angle through the thickness of the core, no assumptions are made here with regards to the pattern of the deformation fields. These fields stem from the formulation of the model, whereas a linear distribution is only assumed for the velocities and accelerations through the thickness of the core. This assumption was also adopted in [28] (as well as in [6]).

3. *Dynamic Governing Equations*

The dynamic governing equations are derived using the equations of motion [Eqs. (11–16)], the constitutive relations [Eqs. (17–20)], the compatibility requirements of the longitudinal deformations at the lower core-sheet interface [Eq. (8b)], and the transverse shear and transverse normal stress fields [Eqs. (21) and (26)]. These equations are stated in terms of the unknown displacements $w_t(x,t)$, $w_b(x,t)$, $u_{ot}(x,t)$, $u_{ob}(x,t)$, and the unknown transverse shear stress $\tau^c(x,t)$, and take the following form (also see [35]) (for brevity, the notation of the independent variables is omitted):

$$bA^t_{xx}u_{ot,xx} - bB^t_{xx}w_{t,xxx} + b\tau^c - m_t\ddot{u}_{ot} + \frac{m_c}{6}\left(h_t\ddot{w}_{t,x} - \frac{1}{2}h_b\ddot{w}_{b,x} - 2\ddot{u}_{ot} - \ddot{u}_{ob}\right) + n_{xt} = 0 \tag{29}$$

$$bA^b_{xx}u_{ob,xx} - bB^b_{xx}w_{b,xxx} - b\tau^c - m_b\ddot{u}_{ob} + \frac{m_c}{6}\left(\frac{1}{2}h_t\ddot{w}_{t,x} - h_b\ddot{w}_{b,x} - \ddot{u}_{ot} - 2\ddot{u}_{ob}\right) + n_{xb} = 0 \tag{30}$$

$$\begin{aligned} &bD^t_{xx}w_{t,xxxx} - bB^t_{xx}u_{ot,xxx} + \frac{bE_c}{h_c}(w_t - w_b) \\ &+ a_1^\sigma\frac{bE_c}{h_c}(\dot{w}_t - \dot{w}_b) - \frac{b\tau^c_{,x}}{2}(h_c + h_t) + m_t\ddot{w}_t - \rho_t I_t\ddot{w}_{t,xx} \\ &+ \frac{m_c h_t}{12}\left(\frac{2\ddot{w}_b + 4\ddot{w}_t}{h_t} - h_t\ddot{w}_{t,xx} + \frac{h_b}{2}\ddot{w}_{b,xx} + 2\ddot{u}_{ot,x} + \ddot{u}_{ob,x}\right) \\ &- q_{zt} + m_{yt,x} = 0 \end{aligned} \tag{31}$$

$$\begin{aligned} &bD^b_{xx}w_{b,xxxx} - bB^b_{xx}u_{ob,xxx} - \frac{bE_c}{h_c}(w_t - w_b) \\ &- a_1^\sigma\frac{bE_c}{h_c}(\dot{w}_t - \dot{w}_b) - \frac{b\tau^c_{,x}}{2}(h_c + h_b) + m_b\ddot{w}_b - \rho_b I_b\ddot{w}_{b,xx} \\ &+ \frac{m_c h_b}{12}\left(\frac{2\ddot{w}_t + 4\ddot{w}_b}{h_b} + \frac{h_t}{2}\ddot{w}_{t,xx} - h_b\ddot{w}_{b,xx} - 2\ddot{u}_{ob,x} - \ddot{u}_{ot,x}\right) \\ &+ q_{zb} + m_{yb} = 0 \end{aligned} \tag{32}$$

$$u_{ot} - u_{ob} + a_1^\tau(\dot{u}_{ot} - \dot{u}_{ob}) - \frac{(h_c + h_t)}{2}w_{t,x} - a_1^\tau\frac{(h_c + h_t)}{2}\dot{w}_{t,x} - \frac{(h_c + h_b)}{2}w_{b,x} - a_1^\tau\frac{(h_c + h_b)}{2}\dot{w}_{b,x} + \frac{\tau^c h_c}{G_c} - \frac{\tau^c_{,xx}h_c^3}{12E_c} = 0 \tag{33}$$

4. *Boundary and Initial Conditions*

The boundary conditions are

$$\lambda N^k_{xx}(t) = \bar{N}_k(t) \quad \text{or} \quad u_{ok}(t) = \bar{u}_{ok}(t) \tag{34}$$

$$-\lambda M^k_{xx}(t) = \bar{M}_k(t) \quad \text{or} \quad w_{k,x}(t) = \bar{w}_{k,x}(t) \tag{35}$$

$$\begin{aligned} \lambda\Big[&M^k_{xx,x}(t) + \tau^c(t)b\frac{h_k}{2} + \rho_k I_k\ddot{w}_{k,x}(t) - \frac{m_c}{24}h_b h_t[\alpha\ddot{w}_{b,x}(t) \\ &- (1-\alpha)\ddot{w}_{t,x}(t)] + \frac{m_c}{24}h_k^2\ddot{w}_{k,x}(t) - \frac{m_c}{6}[\alpha h_t\ddot{u}_{ot}(t) \\ &- (1-\alpha)h_b\ddot{u}_{ob}(t)] - \frac{m_c}{12}[\alpha h_b\ddot{u}_{ob}(t) \\ &- (1-\alpha)h_t\ddot{u}_{ot}(t)] - m_{yk}\Big] = \bar{P}_k(t) \quad \text{or} \quad w_k(t) = \bar{w}_k(t) \end{aligned} \tag{36}$$

$$\tau^c(t) = 0 \quad \text{or} \quad w_c(z_c,t) = \bar{w}_c(z_c,t) \tag{37}$$

where $\bar{P}_k(t)$, $\bar{N}_k(t)$, and $\bar{M}_k(t)$ $(k = t,\ b)$ are dynamic loads and bending moments exerted at the boundaries, $\bar{u}_{ok}(t)$, $\bar{w}_k(t)$, and $\bar{w}_{k,x}(t)$ $(k = 1,\ 2)$ are prescribed deformations and rotations at the boundaries, $\lambda = 1$ where $x = L$, $\lambda = -1$ where $x = 0$, $\alpha = 1$ where $k = t$, $\alpha = 0$ where $k = b$, and $\bar{w}_c(z_c,t)$ is a prescribed deformation field through the height of the core.

The initial conditions at $t = 0$ are

$$u_{oi}(x,0) = \bar{u}_{oi}(x) \qquad (i = t,b) \tag{38}$$

$$\dot{u}_{oi}(x,0) = \bar{\dot{u}}_{oi}(x) \qquad (i = t,b) \tag{39}$$

$$w_i(x,0) = \bar{w}_i(x) \qquad (i = t,b) \tag{40}$$

$$\dot{w}_i(x,0) = \bar{\dot{w}}_i(x) \qquad (i = t,b) \tag{41}$$

where $\bar{u}_{oi}(x)$, $\bar{w}_i(x)$, $\bar{\dot{u}}_{oi}(x)$, $\bar{\dot{w}}_i(x)$ $(i = t,\ b)$ are prescribed displacement and velocity distributions along the beam at $t = 0$.

B. Maxwell's Model

1. *Constitutive Relations*

The classical form of the constitutive relations according to Maxwell's model of viscoelasticity with a single retardation time is

$$\dot{\varepsilon}^c_{zz}(x,z_c,t) = \frac{\dot{\sigma}^c_{zz}(x,z_c,t)}{E_c} + \frac{\sigma^c_{zz}(x,z_c,t)}{b_1^\sigma E_c} \tag{42}$$

$$\dot{\gamma}^c_{xz}(x,z_c,t) = \frac{\dot{\tau}^c_{xz}(x,z_c,t)}{G_c} + \frac{\tau^c_{xz}(x,z_c,t)}{b_1^\tau G_c} \tag{43}$$

where b_1^σ and b_1^τ are the viscous constants of Maxwell's model. The assumptions made in the previous section on the viscous constants (frequency independent within the examined range of response frequencies, constant temperature, no temperature rise due to damping) are adopted here as well. Integration of Eqs. (42) and (43) in time yields the following constitutive relations:

$$\varepsilon_{zz}^c(x,z_c,t)=\frac{\sigma_{zz}^c(x,z_c,t)}{E_c}+\int_0^t\frac{\sigma_{zz}^c(x,z_c,t')}{b_1^\sigma E_c}\,\mathrm{d}t' \tag{44}$$

$$\gamma_{xz}^c(x,z_c,t)=\frac{\tau_{xz}^c(x,z_c,t)}{G_c}+\int_0^t\frac{\tau_{xz}^c(x,z_c,t')}{b_1^\tau G_c}\,\mathrm{d}t' \tag{45}$$

Opposed to the Kelvin–Voigt model, this form shows that Maxwell's model carries a memory of the stressing history in the form of the temporal integrals.

2. *Stress and Displacement Fields*

The transverse shear and transverse normal stresses, Eqs. (21) and (22), directly stem from the requirement of differential equilibrium. Therefore, they are independent of the constitutive behavior and are valid here as well. On the other hand, the transverse displacement, which is determined by means of integration of Eq. (44) through the height of the core, reads

$$w_c(x,z_c,t)=\frac{\{[-\tau_{,x}^c(x,t)z_c^2/2]+C_\sigma(x,t)z_c\}}{E_c}+C_w(x,t)+\frac{[(-z_c^2/2)\int_0^t\tau_{,x}^c(x,t')\,\mathrm{d}t'+z_c\int_0^t C_\sigma(x,t')\,\mathrm{d}t']}{b_1^\sigma E_c} \tag{46}$$

The function $C_w(x,t)$ is determined using the compatibility condition of the transverse displacements at the upper core–face sheet interface [Eqs. (7a)]. Therefore, the distribution of the transverse displacement through the height of the core reads

$$w_c(x,z_c,t)=\frac{\{[-\tau_{,x}^c(x,t)z_c^2/2]+C_\sigma(x,t)z_c\}}{E_c}+\frac{[(-z_c^2/2)\int_0^t\tau_{,x}^c(x,t')\,\mathrm{d}t'+z_c\int_0^t C_\sigma(x,t')\,\mathrm{d}t']}{b_1^\sigma E_c}+w_t(x,t) \tag{47}$$

The function $C_\sigma(x,t)$ is determined using the compatibility condition of the transverse displacements at the lower core–face sheet interface [Eqs. (8a)]. However, due to the implicit integral expressions in Eq. (47), this compatibility condition is to be fulfilled simultaneously with the solution of the governing equations. In other words, the compatibility condition of the transverse deformations at the lower core–face sheet interface [Eq. (8a)] joins the set of governing equations and the additional unknown function $C_\sigma(x,t)$ is added to the set of unknowns.

The distribution of the longitudinal displacement is determined using the kinematic relation [Eq. (5b)] and the constitutive relation [Eq. (45)] and reads

$$u_c(x,z_c,t)=\int\frac{\tau^c(x,t)}{G_c}\,\mathrm{d}z_c+\iint_0^t\frac{\tau^c(x,t')}{b_1^\tau G_c}\,\mathrm{d}t'\,\mathrm{d}z_c-\int w_{c,x}(x,z_c,t)\,\mathrm{d}z_c+C_u(x,t) \tag{48}$$

Substituting the transverse deformation field [Eq. (47)] into Eq. (48), integrating through the height of the core, and using the condition of compatibility of longitudinal displacements at the upper interface [Eq. (7b)] yields the following expression for the longitudinal displacement field:

$$u_c(x,z_c,t)=\frac{z_c\tau^c(x,t)}{G_c}+\int_0^t\frac{z_c\tau^c(x,t')}{b_1^\tau G_c}\,\mathrm{d}t'+\frac{\tau_{,xx}^c(x,t)z_c^3}{6E_c}-\frac{C_{\sigma,x}(x,t)z_c^2}{2E_c}+\frac{z_c^3}{6b_1^\sigma E_c}\int_0^t\tau_{,xx}^c(x,t')\,\mathrm{d}t'-\frac{z_c^2}{2b_1^\sigma E_c}\int_0^t C_{\sigma,x}(x,t')\,\mathrm{d}t'-z_c w_{t,x}(x,t)+u_{ot}(x,t)-\frac{h_t}{2}w_{t,x}(x,t) \tag{49}$$

3. *Dynamic Governing Equations*

The dynamic governing equations are derived using the equations of motion [Eqs. (11–16)], the constitutive relations [Eqs. (17), (18), (44), and (45)], the compatibility requirements of the transverse and longitudinal displacements at the lower core-sheet interface [Eqs. (8a) and (8b)], and the transverse shear and transverse normal stress fields [Eqs. (21) and (22)]. These equations are stated in terms of the unknown displacements $w_t(x,t)$, $w_b(x,t)$, $u_{ot}(x,t)$, $u_{ob}(x,t)$, the unknown transverse shear stress $\tau^c(x,t)$, and the unknown function $C_\sigma(x,t)$, and take the following form (for brevity, the notation of the independent variables is omitted):

$$bA_{xx}^t u_{ot,xx}-bB_{xx}^t w_{t,xxx}+b\tau^c-m_t\ddot{u}_{ot}+\frac{m_c}{6}\left(h_t\ddot{w}_{t,x}-\frac{1}{2}h_b\ddot{w}_{b,x}-2\ddot{u}_{ot}-\ddot{u}_{ob}\right)+n_{xt}=0 \tag{50}$$

$$bA_{xx}^b u_{ob,xx}-bB_{xx}^b w_{b,xxx}-b\tau^c-m_b\ddot{u}_{ob}+\frac{m_c}{6}\left(\frac{1}{2}h_t\ddot{w}_{t,x}-h_b\ddot{w}_{b,x}-\ddot{u}_{ot}-2\ddot{u}_{ob}\right)+n_{xb}=0 \tag{51}$$

$$bD_{xx}^t w_{t,xxxx}-bB_{xx}^t u_{ot,xxx}-b\frac{h_t}{2}\tau^c-bC_\sigma+m_t\ddot{w}_t-\rho_t I_t\ddot{w}_{t,xx}+\frac{m_c h_t}{12}\left(\frac{2\ddot{w}_b+4\ddot{w}_t}{h_t}-h_t\ddot{w}_{t,xx}+\frac{h_b}{2}\ddot{w}_{b,xx}+2\ddot{u}_{ot,x}+\ddot{u}_{ob,x}\right)-q_{zt}+m_{yt,x}=0 \tag{52}$$

$$bD_{xx}^b w_{b,xxxx}-bB_{xx}^b u_{ob,xxx}-b\frac{h_b}{2}\tau^c+bC_\sigma+m_b\ddot{w}_b-\rho_b I_b\ddot{w}_{b,xx}+\frac{m_c h_b}{12}\left(\frac{2\ddot{w}_t+4\ddot{w}_b}{h_b}+\frac{h_t}{2}\ddot{w}_{t,xx}-h_b\ddot{w}_{b,xx}-2\ddot{u}_{ob,x}-\ddot{u}_{ot,x}\right)+q_{zb}+m_{yb}=0 \tag{53}$$

$$\frac{[(-\tau_{,x}^c h_c^2/2)+C_\sigma h_c]}{E_c}+\frac{[(-h_c^2/2)\int_0^t\tau_{,x}^c\,\mathrm{d}t'+h_c\int_0^t C_\sigma\,\mathrm{d}t']}{b_1^\sigma E_c}+w_t-w_b=0 \tag{54}$$

$$\frac{h_c\tau^c}{G_c}+\frac{h_c}{b_1^\tau G_c}\int_0^t\tau^c\,\mathrm{d}t'+\frac{\tau_{,xx}^c h_c^3}{6E_c}-\frac{C_{\sigma,x}h_c^2}{2E_c}+\frac{h_c^3}{6b_1^\sigma E_c}\int_0^t\tau_{,xx}^c\,\mathrm{d}t'-\frac{h_c^2}{2b_1^\sigma E_c}\int_0^t C_{\sigma,x}\,\mathrm{d}t'-h_c w_{t,x}+u_{ot}-Y_t w_{t,x}-u_{ob}-Y_b w_{t,x}=0 \tag{55}$$

Note that Eqs. (54) and (55), which result from the compatibility requirements of the transverse and longitudinal deformations at the lower core-sheet interface [Eqs. (8a) and (8b)], respectively, include the integral history terms.

4. *Boundary and Initial Conditions*

Also here, seven time-dependent boundary conditions are prescribed at the ends of the beam, and two x-dependent initial conditions at $t=0$ are defined for each of the four unknown

displacements. According to the principle of virtual work, Eq. (1), the unknown function $C_\sigma(x,t)$, which is only defined in the field, is not subjected to boundary conditions. In addition, at time $t=0$, the temporal integrals vanish and $C_\sigma(x,0)$, which is obtained from Eq. (54), is not subjected to initial conditions. Hence, the boundary and initial conditions of Maxwell's model are identical to those of the Kelvin–Voigt model of Eqs. (34–41).

III. Solution

Each of the two sets of dynamic governing equations [Eqs. (29–33) and Eqs. (50–55)] form a set of partial differential equations. The solution of the governing equations in time uses Newmark's approach [38]. The time domain is divided into finite intervals and the first and second time derivatives of each unknown function are expressed as explicit functions of the unknowns in the present time step and the known functions and their first and second time derivatives in the preceding time step. Thus, the first and second time derivatives of a generic unknown function $g(x,t)$ at the end of the jth time step ($t=t_j$) take the following form:

$$\dot g(x,t_j)\equiv \dot g(x)_j=\frac{(\beta\Delta t-\gamma\Delta t)\dot g(x)_{j-1}+\gamma[g(x)_j-g(x)_{j-1}]+(\beta\Delta t^2-\frac{1}{2}\gamma\Delta t^2)\ddot g(x)_{j-1}}{\beta\Delta t} \tag{56}$$

$$\ddot g(x,t_j)\equiv \ddot g(x)_j=\frac{g(x)_j-g(x)_{j-1}-\Delta t\dot g(x)_{j-1}-\frac{1}{2}\Delta t^2\ddot g(x)_{j-1}+\beta\Delta t^2\ddot g(x)_{j-1}}{\beta\Delta t^2} \tag{57}$$

where $\ddot g(x)_j$, $\dot g(x)_j$, and $g(x)_j$ are unknown functions at the jth time step, $\ddot g(x)_{j-1}$, $\dot g(x)_{j-1}$, and $g(x)_{j-1}$ are known functions at the end of the $j-1$th time step (with $t_0=0$), β and γ are parameters that control the stability and accuracy characteristics of the algorithm, and Δt is the time step interval.

By using this procedure, the governing equations that are based on the Kelvin–Voigt model [Eqs. (29–33)] reduce to a set of ordinary differential equations (ODEs) in terms of the unknowns $w_t(x)_j$, $w_b(x)_j$, $u_{ot}(x)_j$, $u_{ob}(x)_j$, and $\tau^c(x)_j$. These equations, along with the boundary conditions, are solved analytically or numerically at every time step. Here, a multiple shooting method (e.g., Stoer and Bulirsch [39]) is adopted.

On the other hand, by applying the preceding procedure to the governing equations that are based on Maxwell's model [Eqs. (50–55)], the equations still include implicit time integrals that require special treatment. Based on Newmark's approach [38], the time integrals in Eqs. (54) and (55) are also expressed as explicit functions of the unknowns in the present time step and the known functions, their first time derivatives, and their second time derivatives in the preceding time step. Recalling Newmark's method,

$$g(x,t_j)\equiv g(x)_j=g(x)_{j-1}+\Delta t\dot g(x)_{j-1}+\frac{\Delta t^2}{2}[(1-2\beta)\ddot g(x)_{j-1}+2\beta\ddot g(x)_j] \tag{58}$$

The integral of $g(x)$ at time $t=t_j$ becomes

$$\int_0^{t_j} g(x,t')\,dt'=\int_0^{t_{j-1}} g(x,t')\,dt'+\Delta t g(x)_{j-1}+\frac{\Delta t^2}{2}\dot g(x)_{j-1}+\frac{\Delta t^3}{6}[(1-2\beta)\ddot g(x)_{j-1}+2\beta\ddot g(x)_j] \tag{59}$$

By substituting Eq. (57) into Eq. (59), the integral of any unknown function $g(x)$ at time $t=t_j$ becomes a function of the unknown function at the present time $g(x)_j$, the known integral of this function from $t=0$ to $t=t_{j-1}$, and the known function and its first time derivative at $t=t_{j-1}$, as follows:

$$\int_0^{t_j} g(x,t')\,dt'=\int_0^{t_{j-1}} g(x,t')\,dt'+\frac{\Delta t}{3}g(x)_j+\frac{2\Delta t}{3}g(x)_{j-1}+\frac{\Delta t^2}{6}\dot g(x)_{j-1} \tag{60}$$

Using this procedure, Eqs. (50–55) reduce to a set of algebraic-differential equations in terms of $w_t(x)_j$, $w_b(x)_j$, $u_{ot}(x)_j$, $u_{ob}(x)_j$, $\tau^c(x)_j$, and $C_\sigma(x)_j$. The last term $C_\sigma(x)_j$ is eliminated from the evolution of Eq. (54) and is introduced into the evolution of Eq. (55) to yield a set of ODEs that is compatible with the boundary conditions of Eqs. (34–37). Also here, a multiple shooting method, which is described next, is adopted for the resulting equations.

In the multiple shooting method, the governing equations that are based on the Kelvin–Voigt model [Eqs. (29–33)] or Maxwell's model [Eqs. (50–55)] are first converted into a set of ordinary first-order differential equations in terms of the unknown deformations, slopes, internal forces, shear stress, and shear stress gradient. In the following discussion, the unknowns are designated by the entries of the unknown vector $\mathbf{Y}(x)$. The spatial domain $x=[0,L]$ is then divided into N regions, and the set of first-order equations is numerically integrated using the Runge–Kutta or other method with assumed initial conditions s_m^n in each region:

$$s_m^n=\mathbf{Y}_m(x_n),\qquad m=1,\ldots,M,\qquad n=1,\ldots,N \tag{61}$$

where M is the number of first-order governing equations (in the present case $M=14$), s_m^n is the assumed initial value for the mth unknown function in the nth region, and x_n is the x coordinate of the left end of the nth region. The numerical solution of the differential equations is reduced to finding the vector s_m^n that satisfies $F(s_m^n)=0$, where F stands for the difference between the value of s_m^n at the left end of the nth region and the value at the right end of the adjacent region (nth -1) resulting from the numerical integration, the differences between s_m^1 and the prescribed values given by the boundary conditions at the left end of the beam, and the differences between the values at the right end of the Nth region resulting from the numerical integration and the prescribed values given by the boundary conditions at the right end of the beam. In general, the unknowns s_m^n that satisfy all continuity and boundary conditions are iteratively solved for using the Newton–Raphson scheme. However, in linear problems, the multiple shooting method yields a simpler straightforward solution procedure; see, for example, Stoer and Bulirsch [39].

IV. Advanced Viscoelastic Models

The two fundamental viscoelastic models (as well as the elastic solid model [6] and the viscous fluid model which is not addressed here) and their analytical and numerical treatment provide a basis and building blocks for more refined viscoelastic models that include multiple retardation times or multiple rheologic components. To illustrate this, consider the generalized Maxwell viscoelastic model for the core that includes a number of Maxwell units and a single Hookean (elastic) spring connected in parallel. Each viscoelastic unit has different material constants and relaxation time. In this case, and in any desired viscoelastic model, the equations of motion [Eqs. (11–16)], which are not affected by the constitutive relation, do not

change. On the other hand, the stresses in the core equal to the sum of stresses developed in each unit

$$\sigma^c_{zz}(x,z_c,t)=\sum_{u=1}^{\tilde{N}}\sigma^c_{zzu}(x,z_c,t);\qquad \tau^c_{xz}(x,z_c,t)=\sum_{u=1}^{\tilde{N}}\tau^c_{xzu}(x,z_c,t) \tag{62}$$

where $\tilde{N}$ is the number of units in parallel. Recalling Maxwell's constitutive relations [Eqs. (44) and (45)] and using Eq. (60), the transverse normal strain and shear angle at the uth Maxwell's unit, which are equal to those of the entire group, take the following form:

$$\begin{aligned}\varepsilon^c_{zz}(x,z_c,t_j)&=\frac{\sigma^c_{zzu}(x,z_c,t_j)}{E_{cu}}+\frac{\Delta t}{3}\frac{\sigma^c_{zzu}(x,z_c,t_j)}{b^\sigma_u E_{cu}}\\&+\int_o^{t_{j-1}}\frac{\sigma^c_{zzu}(x,z_c,t')}{b^\sigma_u E_{cu}}\,\mathrm{d}t'+\frac{2\Delta t}{3}\frac{\sigma^c_{zzu}(x,z_c,t_{j-1})}{b^\sigma_u E_{cu}}\\&+\frac{(\Delta t)^2}{6}\frac{\dot\sigma^c_{zzu}(x,z_c,t_{j-1})}{b^\sigma_u E_{cu}}\end{aligned} \tag{63}$$

$$\begin{aligned}\gamma^c_{xz}(x,z_c,t_j)&=\frac{\tau^c_{xzu}(x,z_c,t_j)}{G_{cu}}+\frac{\Delta t}{3}\frac{\tau^c_{xzu}(x,z_c,t_j)}{b^\tau_u G_{cu}}\\&+\int_o^{t_{j-1}}\frac{\tau^c_{xzu}(x,z_c,t')}{b^\tau_u G_{cu}}\,\mathrm{d}t'+\frac{2\Delta t}{3}\frac{\tau^c_{xzu}(x,z_c,t_{j-1})}{b^\tau_u G_{cu}}\\&+\frac{(\Delta t)^2}{6}\frac{\dot\tau^c_{xzu}(x,z_c,t_{j-1})}{b^\tau_u G_{cu}}\end{aligned} \tag{64}$$

where E_{cu} and G_{cu} are the transverse modulus of elasticity and shear modulus of the uth unit, and b^σ_u and b^τ_u are the viscous constants of the uth unit. These constants, as well as the material moduli and the assumed relaxation time of each unit, can be determined by a Prony or Dirichlet series with the aid of the least square or other method to fit test data. The normal strain and shear angle of the $\tilde{N}$th unit, which correspond to the single Hookean spring, can be degenerated from Eqs. (63) and (64) by setting the viscous terms ($1/b^\sigma_{\tilde{N}}$ and $1/b^\tau_{\tilde{N}}$) to zero. Also note that, for $\tilde{N}=2$, Eqs. (62–64) recover the standard linear solid model that combines a single Maxwell unit and a Hookean spring in parallel.

As all the terms that are related to the response at time $t=t_{j-1}$ are known, the stresses at time $t=t_j$ can be obtained from Eqs. (63) and (64) in terms of the unknown normal strains and shear angles at $t=t_j$, and the known response at $t=t_{j-1}$. These stresses are then backsubstituted into Eq. (62) to obtain the general constitutive relations of the generalized Maxwell model at each time step. Following the procedure described in Sec. II.B, the stress and displacement fields in the core layer, as well as the governing equations, are then obtained. For brevity, this is not described here, however, note that, once the solution is known at $t=t_j$, the stresses at each unit can be obtained using Eqs. (63) and (64).

V. Numerical Study

The numerical study examines the influence of the viscoelastic characteristics of the core layer and compares the theoretical results with experimental ones available in the literature. The first example focuses on the behavior of an ordinary sandwich beam that is simply supported at the ends of its faces and at the core. The second example focuses on the behavior of a sandwich beam simply supported at the lower face sheet and free at the upper face sheet and the core. The third example studies the behavior of the cantilevered sandwich beam that was experimentally studied by Barbosa and Farage [40].

A. Sandwich Beam Simply Supported at the Ends

The geometry, mechanical properties, and the dynamic load appear in Fig. 2. Although this sandwich beam includes a relatively thin core, where the transverse deformation and dissipation may be negligible, it is provided here to describe and explain some of the main differences between the two viscoelastic models. The shear modulus of the core and its corresponding modulus of elasticity are taken from Galucio et al. [16], assuming that the vibration frequency of the structure equals its first natural frequency (76 Hz), which was obtained by a preliminary free vibration analysis. The viscoelastic coefficients of the core material used in the Kelvin–Voigt model are estimated as $a^\tau_1=\eta_\tau/\omega$ and $a^\sigma_1=\eta_\sigma/\omega$ (see [35]), where η_τ and η_σ are the core material loss factors in shear and normal stresses, respectively (see [41]), and ω is the frequency. Following Galucio et al. [16], the magnitudes of the loss factors for 3M ISD112 material at room temperature and at a frequency level of approximately 76 Hz are estimated as $\eta_\tau=\eta_\sigma=10^{-5}$. Thus, the viscous coefficients are taken as $a^\tau_1=a^\sigma_1=0.00066$ s. For reference, the peak deflections of the face sheets (at midspan) and the peak transverse shear stresses that develop under static loading are $w_b=0.579$ mm, $w_t=0.585$ mm, and $\tau^c=3.168$ kPa.

The time variation of the peak deflections, and the variation of the peak transverse shear stresses under the dynamic step load are studied using the Kelvin–Voigt model for the core [Eqs. (29–33)] in

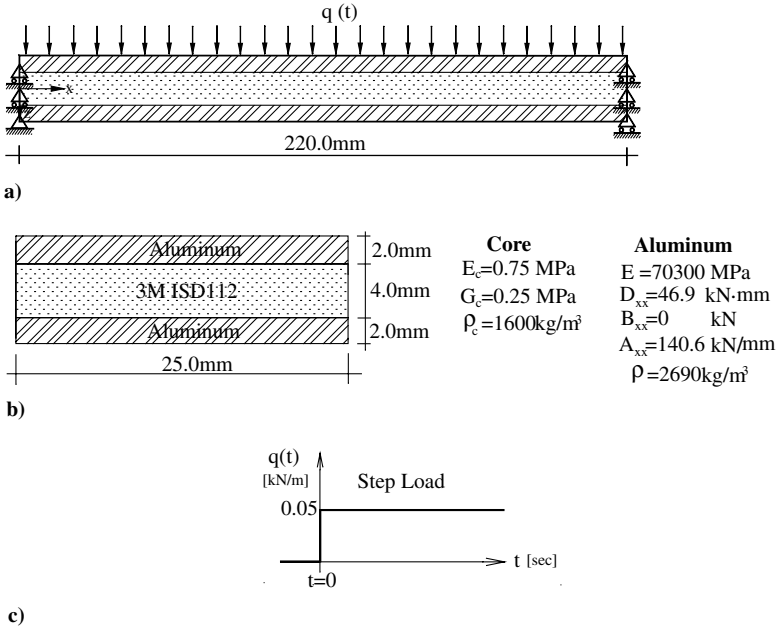

Fig. 2 Geometry, material properties, and loading of an ordinary sandwich beam: a) geometry, b) cross section and material properties, c) step load.

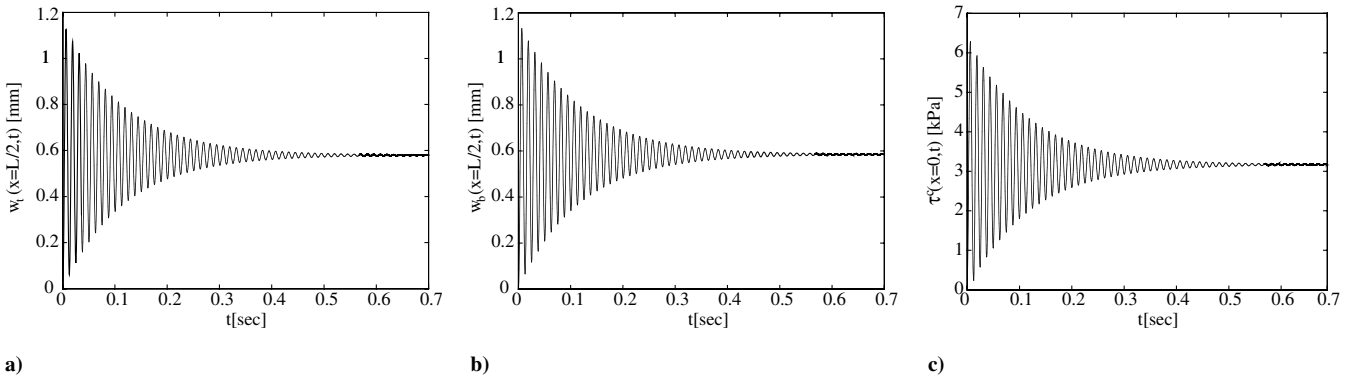

Fig. 3 Response to a step load of a sandwich beam simply supported at both face sheets and the core; Kelvin–Voigt model for the core material: a) deflection of upper face sheet, b) deflection of lower face sheet, c) peak transverse shear stresses.

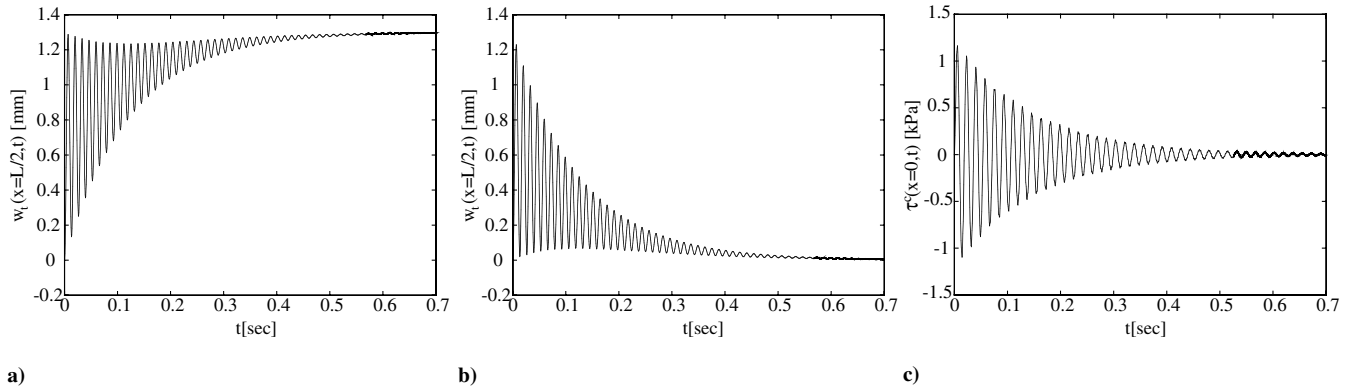

Fig. 4 Response to a step load of a sandwich beam simply supported at both face sheets and the core; Maxwell's model for the core material: a) deflection of upper face sheet, b) deflection of lower face sheet, c) peak transverse shear stresses.

Fig. 3. The results show that the deflections and stresses decay in time toward the elastic static results. It is also shown that the deflections of the upper and lower face sheets are almost identical through the entire time domain. Using the logarithmic decrement technique, the damping ratio in terms of transverse deflections and stresses is about 1.8% of the critical one.

Figure 4 shows the dynamic response of the sandwich beam analyzed using Maxwell's model [Eqs. (50–55)]. In this case, the viscous coefficients were chosen to give the overall damping ratio of 1.8% akin to the one obtained by Kelvin–Voigt model. This equivalency yields $b_1^\sigma = b_1^\tau = 0.001$ s. The results show that, although the structure oscillates with the same frequency as the one obtained in the Kelvin–Voigt model, its behavior in time is significantly different. It can be seen that the transverse deflection of the upper face sheets asymptotically reaches a constant finite displacement, whereas that of the lower face sheet oscillates around an asymptotically decreasing line toward zero. The peak shear stress, on the other hand, oscillates around the zero line and decays in time. These results actually reveal that, although the core layer is modeled as a Maxwell model, the entire sandwich beam behaves like a standard linear solid model that combines the Maxwell model and a Hookean spring in parallel. In this case, the Hookean spring effect is attributed to the bending stiffness of the upper face sheet and its ability to transfer load to the supports. Thus, as the stresses in the core layer and their rate of change decay in time (Fig. 4c), the viscoelastic Maxwell layer becomes less and less effective in terms of resisting the shear

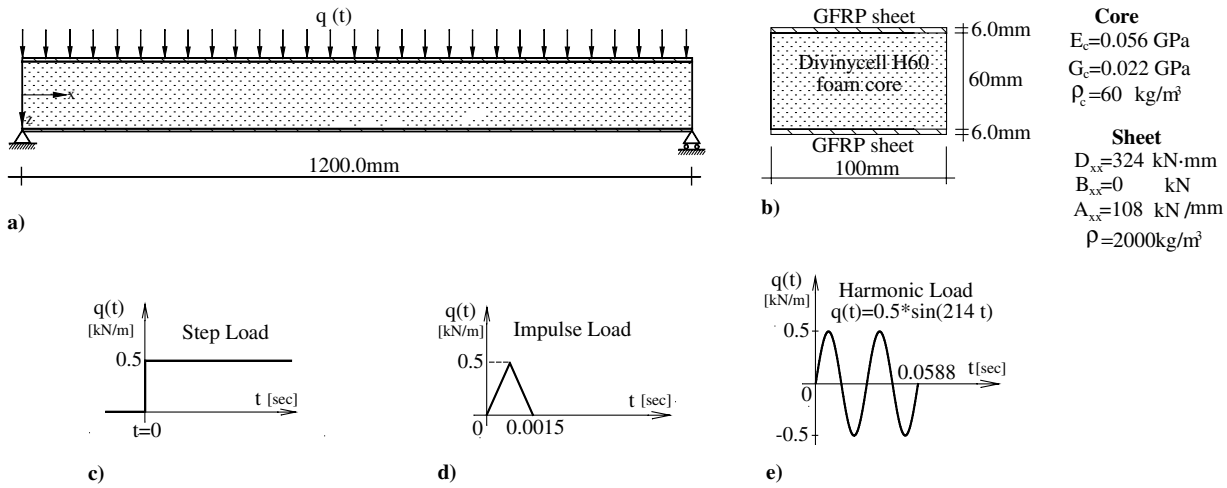

Fig. 5 Geometry, material properties, and loading: a) geometry and cross section, b) material properties, c) step load, d) impulse load, e) harmonic load.

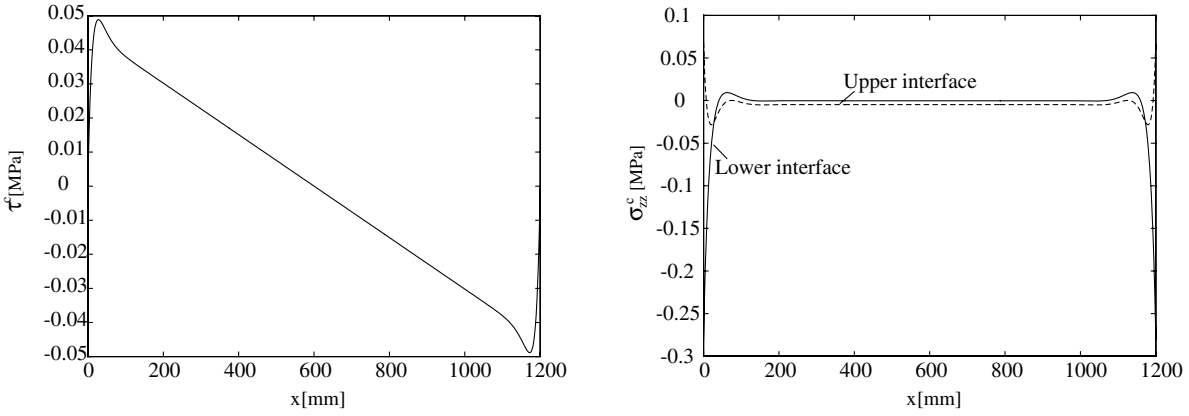

a) b)

Fig. 6 Static response: a) transverse shear stresses in the core, b) transverse normal stresses at the core interfaces.

and transverse normal stresses. A larger portion of the global bending moment is then carried in the form of bending of the loaded face sheet while a smaller part is carried by means of the composite action of the face sheets and the core. Once the internal stresses in the core are fully relaxed, all the external loading is carried through bending of the upper face sheet only, and the finite displacement of the upper face sheet (1.3 mm) actually equals the static elastic displacement of a simply supported beam of the same elastic and geometric properties as the upper sheet. In practical terms, the load resisting mechanism evolving with the Maxwell model is evidently not desired, as the sandwich quickly looses its ability to resist loads through composite action of the face sheets and the core.

Note that, as the viscoelastic feature of the core that is modeled by a Kelvin–Voigt model damps the entire response of the structure, including all the transverse displacements, the core in this case is more effective than the case with Maxwell's model. Because of that, it can be seen in Figs. 3c and 4c that the peak shear stresses that develop with the Kelvin–Voigt viscoelastic core are significantly higher than the ones with Maxwell's model.

B. Sandwich Beam Simply Supported at the Lower Face

The geometry, mechanical properties, and the dynamic loads appear in Fig. 5. The beam consists of two glass fiber reinforced

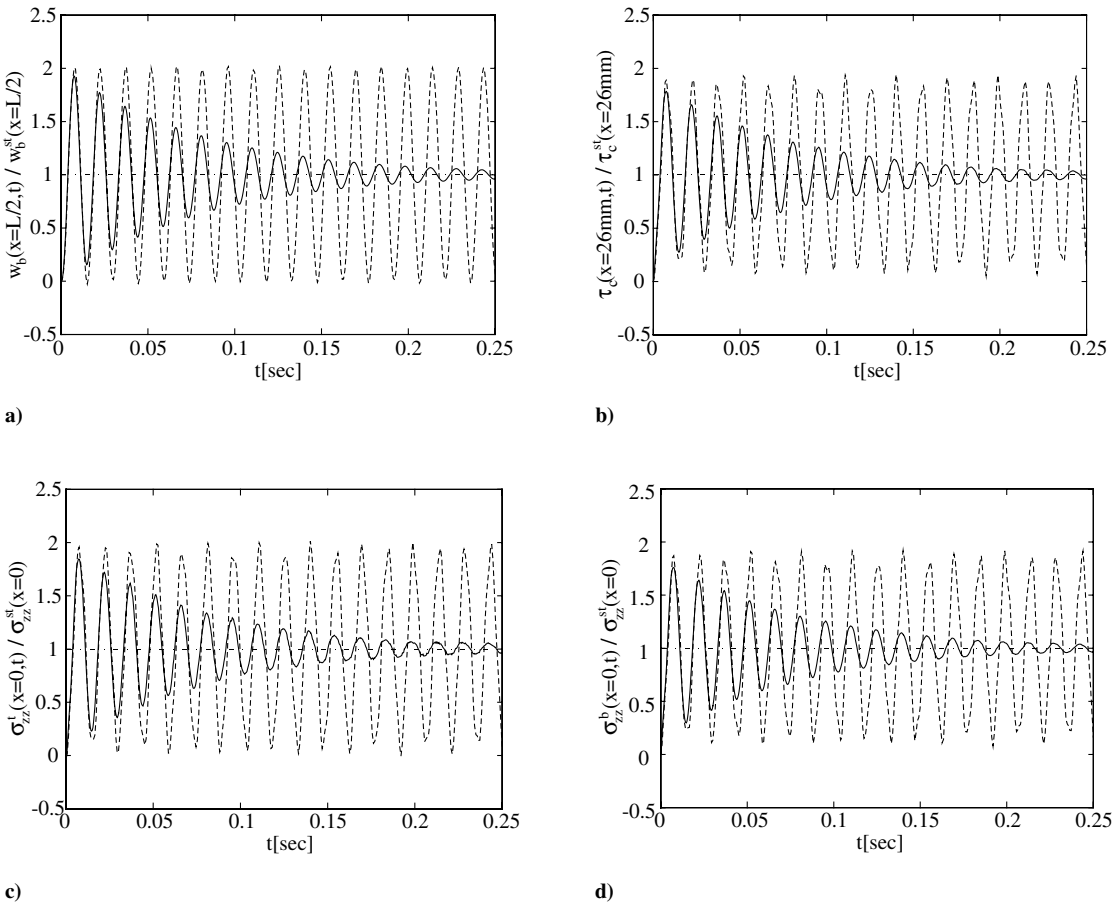

a) b) c) d)

Fig. 7 Response of a sandwich beam supported at the lower face sheet to a step load; Kelvin–Voigt model (solid line: viscoelastic core; dashed line: elastic core): a) deflection, b) peak transverse shear stresses, c) peak transverse normal stresses, upper interface, d) peak transverse normal stresses, lower interface.

polymer (GFRP) face sheets and a Divinycell H60 foam core. Following Dwivedy et al. [5], the magnitudes of the loss factors for Divinycell H60 foam at room temperature are estimated as $\eta_\tau = \eta_\sigma = 0.1$. The first natural frequency of the structure is obtained by a preliminary analysis and equals about 68 Hz. Thus, the viscous coefficients are taken as $a_1^\tau = a_1^\sigma = 0.000234$ s. The step, impulse, and harmonic dynamic loads shown in Fig. 5 are examined. The interfacial stresses that develop in the beam under a static load of equal magnitude appear in Fig. 6 and reveal the transverse shear and transverse normal stress concentrations near the edges and the variation of the normal stresses from one core-face interface to another.

1. Simply Supported (at the Lower Face Sheet) Beam: Response to Step Load

The time variation of the stresses at their critical locations and the variation of the peak deflection at midspan under the step load are studied in Fig. 7 using the Kelvin–Voigt model. The results are normalized with respect to the static elastic results and the figures describe the dynamic magnification factors (DMFs) with DMF = 1 designating the static value. For reference, the response of the sandwich beam with an elastic core ($a_1^\tau = a_1^\sigma = 0$) is plotted in dashed lines. The results show that, with the viscoelastic core, the peak DMF is approximately 1.9 at the first vibration cycle and it decays after few cycles. In the case of the elastic core, the peak DMF does not decay and, as expected, it equals 2.0. The damping ratio in terms of transverse deflections and stresses is about 3% of the critical one. These results quantify the level of effective damping expected with the Kelvin–Voigt type of viscoelastic core.

Figure 8 shows the dynamic response of the sandwich beam analyzed using Maxwell's model. Also here, the viscous coefficients were chosen to give the overall damping ratio of 3% obtained by the Kelvin–Voigt model, to yield $b_1^\tau = b_1^\sigma = 0.018$ s. The results show that the natural frequency and the DMFs of the internal stresses are similar to the ones obtained using the Kelvin–Voigt model. However, in terms of transverse deflection, Fig. 8a shows that Maxwell's model damps the vibratory response but yields a monotonic growth of the deflections in time. Because, in this case, the lower face sheet is supported, its peak deflection (Fig. 8a) eventually approaches a finite value. However, this finite displacement, which is determined by the relatively low flexural rigidity of the lower face sheet only, is about 350 times the static displacement of the entire sandwich beam. This effect is not prominent within the time interval shown in Fig. 8.

In the unique case studied here, the load is applied to the upper face sheet while only the lower face sheet is supported (Fig. 5a). As the rates of the internal stresses diminish in time, the peak levels of transverse shear stresses in the core and interfacial normal stresses at the lower interface slightly drop toward normalized values that are smaller than one (Figs. 8b and 8d). On the other hand, the peak interfacial normal stresses at the upper interface decay toward a normalized value of one. This is attributed to the effect of the external load applied to the upper face sheet, its notable influence on the normal stresses at the upper interface, and the fact that the upper face sheet is not directly supported but transfers the load to the supported lower face sheet through the core. On the other hand, the decay of the shear stresses and the interfacial normal stresses at the lower interface below the level of the static values is a result of the softening effect introduced by Maxwell's model and the corresponding redistribution of stresses in the structure. Under the sustaining load studied here, this effect eventually leads to large deflections of the lower supported face sheet and unbounded deflections of the upper (nonsupported) face sheet. These effects imply that, by itself, Maxwell's model, which is naturally more relevant to viscous fluids, does not provide a realistic representation of the solid core of the partially supported sandwich structure subjected to a sustained load. The importance and

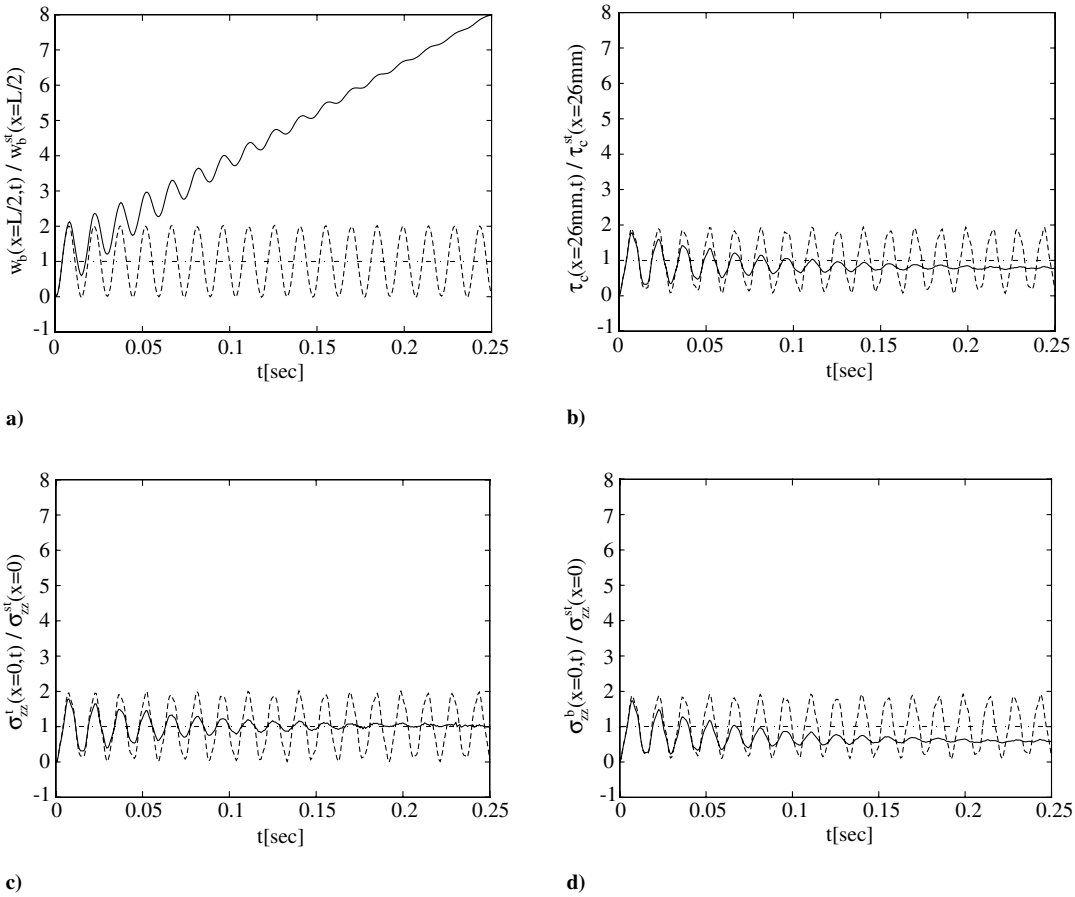

Fig. 8 Response of a sandwich beam supported at the lower face sheet to a step load; Maxwell's model (solid line: viscoelastic core; dashed line: elastic core): a) deflection, b) peak transverse shear stresses, c) peak transverse normal stresses, upper interface, d) peak transverse normal stresses, lower interface.

relevance of Maxwell's model to the problem at hand is due to its role as a building block for refined representation of the viscoelastic nature of the core material and its ability to demonstrate, shed light on, and explain some aspects of the response of the structure.

2. Simply Supported (at the Lower Face Sheet) Beam: Response to Impulse load

The dynamic response of the beam subjected to a triangular impulse load (Fig. 5d) is investigated using the Kelvin–Voigt and Maxwell's models in Fig. 9. The load duration is about one-tenth the first vibration period. Also here, the results are normalized with respect to the response to a static load of equal magnitude, and the results corresponding to the case of the elastic core are included. The elastic and viscoelastic properties are the same as the ones used in the previous case.

The results of the sandwich beam with elastic core show that the time variation of the transverse deflection and transverse shear stresses is controlled by the first mode of the structure but is also influenced by higher vibration modes. Yet, the effect of the higher modes of vibration is less pronounced in the deflection results compared to the stress results. When a Kelvin–Voigt viscoelastic core material is used, the high-frequency effects in the stresses response are rapidly decayed (see Fig. 9b).

The results obtained using Maxwell's model appear in Fig. 9c (deflections) and Fig. 9d (interfacial shear). The comparison between the two models in terms of deflections shows that, in both cases, the vibratory response is effectively damped. However, with the Kelvin–Voigt model (Fig. 9a), the beam oscillates around the zero line, and with Maxwell's model (Fig. 9c), the deflections decay toward a residual value that is slightly higher than that (around 0.02). This nonphysical residual displacement is attributed to a numerical artifact associated with the higher frequency modes. These modes are triggered by the impulse loading but are not effectively damped using a Maxwell model with a single relaxation time. To examine this effect, the behavior of the sandwich beam under a harmonic load that is less involved with the higher frequency modes is studied in Sec. V.B.3. Figure 9d also shows that, with Maxwell's model, the higher frequencies decay much slower and still affect the dynamic response. These differences highlight the importance of the characterization of the viscoelastic properties of the core and the selection of the corresponding model.

3. Simply Supported (at the Lower Face Sheet) Beam: Response to Harmonic Load

The dynamic response of the beam subjected to a harmonic load (Fig. 5e) is investigated in Fig. 10. The frequency of the applied harmonic load equals half the 34 first natural frequency of the beam (34 Hz), and the load duration is 4 times the first vibration period (Fig. 5e). The results are normalized with respect to the response to a static load of equal magnitude.

The results obtained using the Kelvin–Voigt model (Figs. 10a and 10b) reveal that, once the load is released, the response in terms of displacement and transverse shear stress is effectively damped by the viscoelastic core toward zero. Similarly, as this loading history only slightly triggers higher frequency modes, the response according to Maxwell's model (Figs. 10c and 10d) decays toward zero displacement and stresses, with no artificial residual values. Thus, once the higher frequency modes are not significantly triggered (opposed to the impulse loading studied in Fig. 9) Maxwell's model with single relaxation time can better describe the behavior of the structure.

C. Cantilevered Sandwich Beam

The dynamic response of the cantilevered sandwich beam that was theoretically and experimentally studied by Barbosa and Farage [40] is studied here. The geometry, the mechanical properties, and the

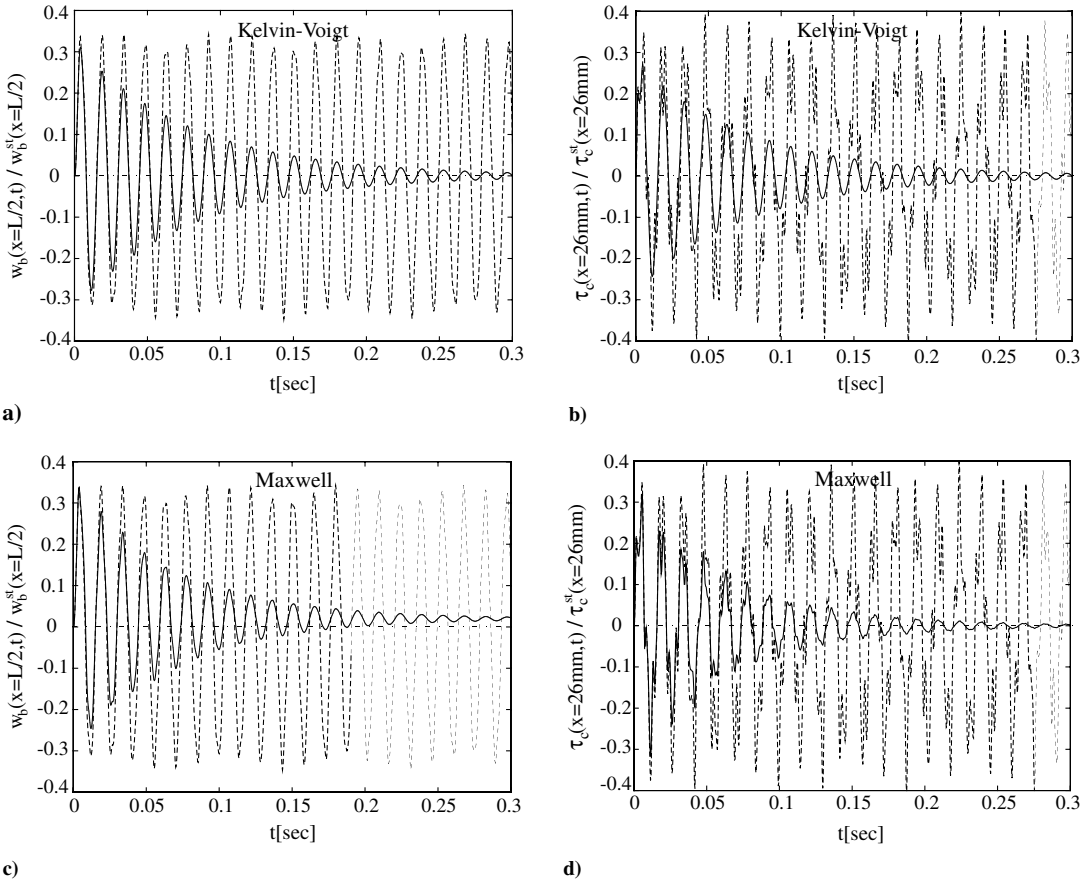

Fig. 9 Response of a sandwich beam supported at the lower face sheet to an impulse load (solid line: viscoelastic core; dashed line: elastic core): a) deflections with Kelvin–Voigt model for the core, b) peak transverse shear stresses with Kelvin–Voigt model for the core, c) deflection with Maxwell's model for the core, d) peak transverse shear stresses with Maxwell's model for the core.

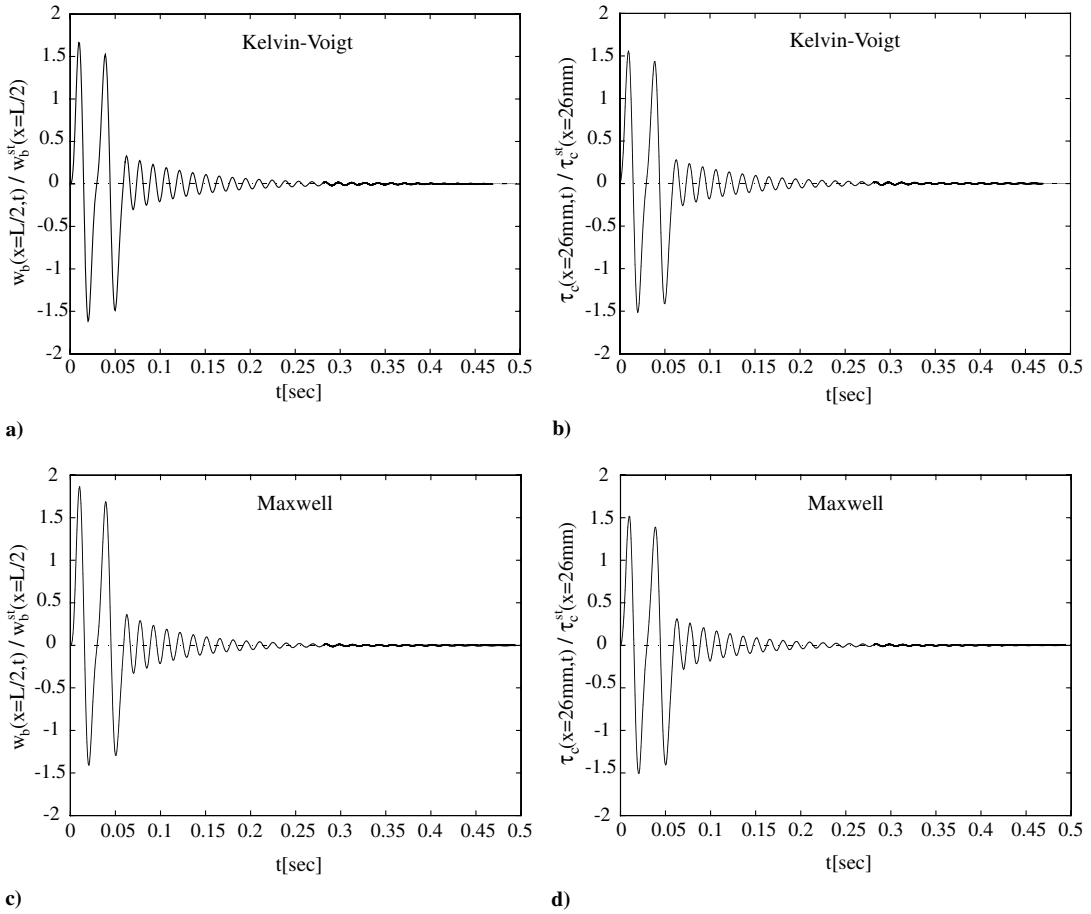

Fig. 10 Response of a sandwich beam supported at the lower face sheet to a harmonic load: a) deflections with Kelvin–Voigt model for the core, b) peak transverse shear stresses with Kelvin–Voigt model for the core, c) deflection with Maxwell's model for the core, d) peak transverse shear stresses with Maxwell's model for the core.

dynamic loads appear in Fig. 11. The boundary conditions at the clamped edge include zero deflections and rotations of the face sheets and zero transverse deflection through the height of the core. The response of the beam to the impulse load (Fig. 11c) that was used and reported in the experimental study [40] is examined. The hammer excitation impact was not measured or reported in [40] and, therefore, the magnitude of the load was evaluated by multiplying the hammer's mass (0.2 kg) by the peak measured acceleration

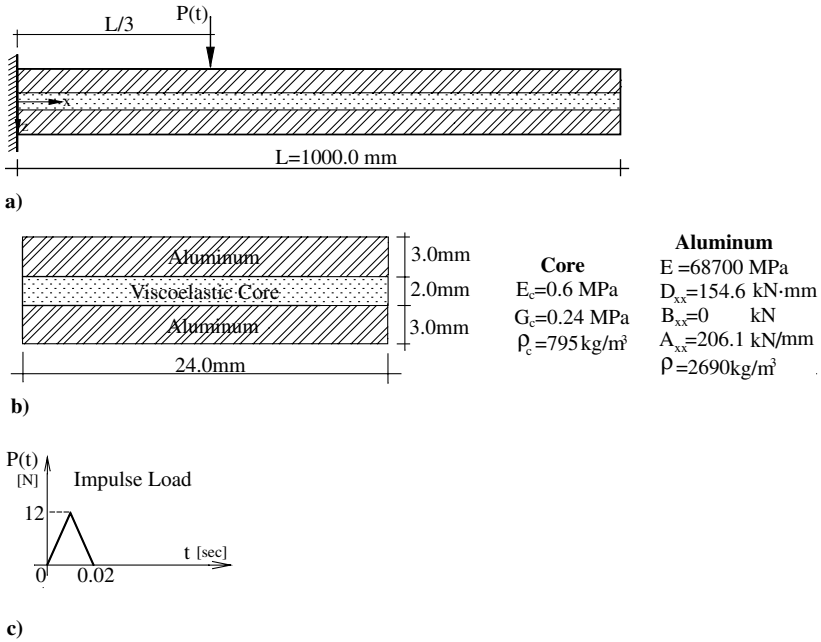

Fig. 11 Geometry, material properties, and loading of a cantilevered sandwich beam (adapted from Barbosa and Farage [40]): a) geometry, b) cross section and material properties, c) impulse load.

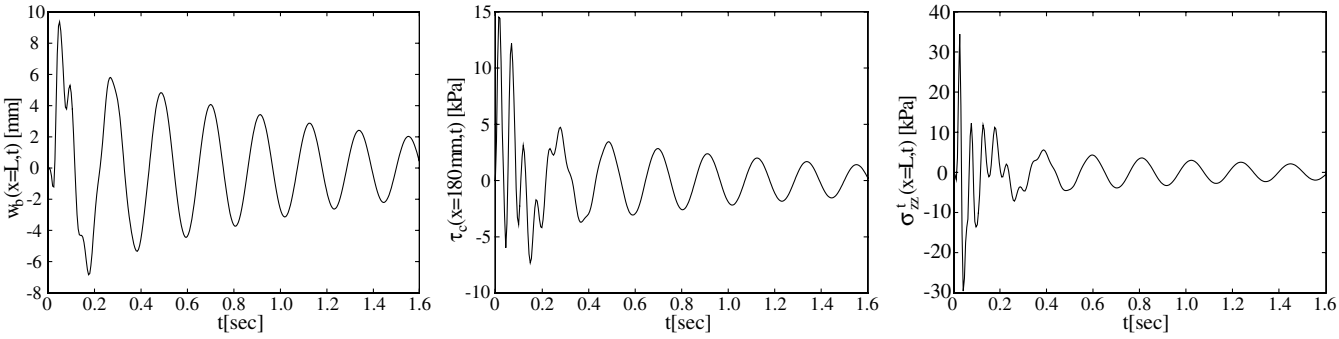

Fig. 12 Theoretical response of a cantilevered sandwich beam to impulse load with Kelvin–Voigt model for the core: a) deflection (lower face sheet), b) peak transverse shear stresses, c) peak transverse normal stresses at the upper interface.

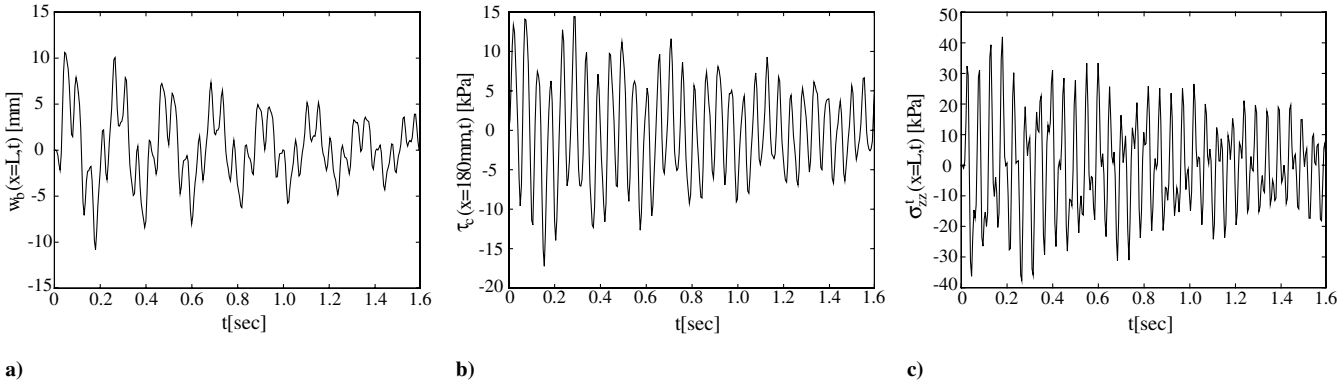

Fig. 13 Theoretical response of a cantilevered sandwich beam to impulse load with Maxwell's model for the core: a) deflection (lower face sheet), b) peak transverse shear stresses, c) peak transverse normal stresses at the upper interface.

(60 m/s^2). The load duration was also approximated from the experimental results as 10% of the vibration period of the structure. Following [40], the magnitude of the overall loss factor for the viscoelastic material obtained from the experimental data is $\eta = 0.1434$, and the natural frequency of the sandwich beam is 5.05 Hz. Because of the absence of more detailed data, it is assumed that the reported loss factors applies to both transverse shear and transverse normal response. Thus, the viscous coefficients according to the Kelvin–Voigt model are taken as $a_1^\sigma = a_1^\tau = 0.0045$ s, whereas those according to Maxwell's model were chosen to give an overall damping ratio of the deflections similar to the one obtained by the Kelvin–Voigt model. This equivalency yields $b_1^\sigma = b_1^\tau = 0.25$ s. In addition, due to the lack of data, it is also assumed that the elastic moduli of the viscoelastic core, which appear in Fig. 11b, are applicable for both the Kelvin–Voigt and the Maxwell model. However, in a more accurate analysis, these parameters should be given different values in the two models, as these parameters depend differently upon the magnitude of the frequency. This aspect is not considered here.

The time response of the peak deflection and peak interfacial stresses obtained by the Kelvin–Voigt model and by Maxwell's model are described in Figs. 12 and 13, respectively. Figure 12 shows that the dominant vibration frequency in terms of transverse deflection and interfacial stresses equals about 4.75 Hz. This value is in fair agreement with the experimental result (5.05 Hz). Note that the impulse load triggers higher modes of vibration but the Kelvin–Voigt viscoelastic core damps these effects and eliminates them after the first cycle of vibration (Fig. 12). With Maxwell's model (Fig. 13), the decay of the higher modes is notably less significant and the higher frequencies are prominent through the entire time domain. The application of the fast Fourier transform to Maxwell's model results shows that the lower among the two dominant frequencies is about

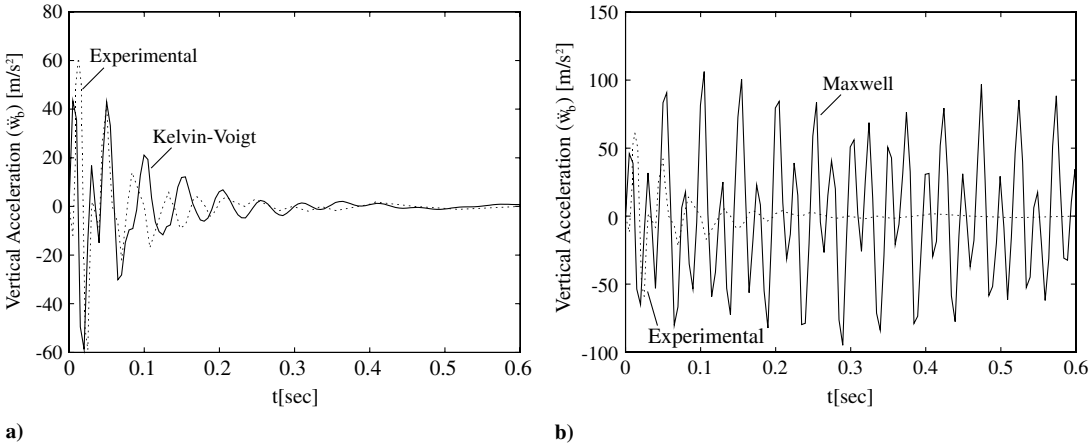

Fig. 14 Theoretical and experimental [40] response to impulse load: a) Kelvin–Voigt model for the core, b) Maxwell's model for the core.

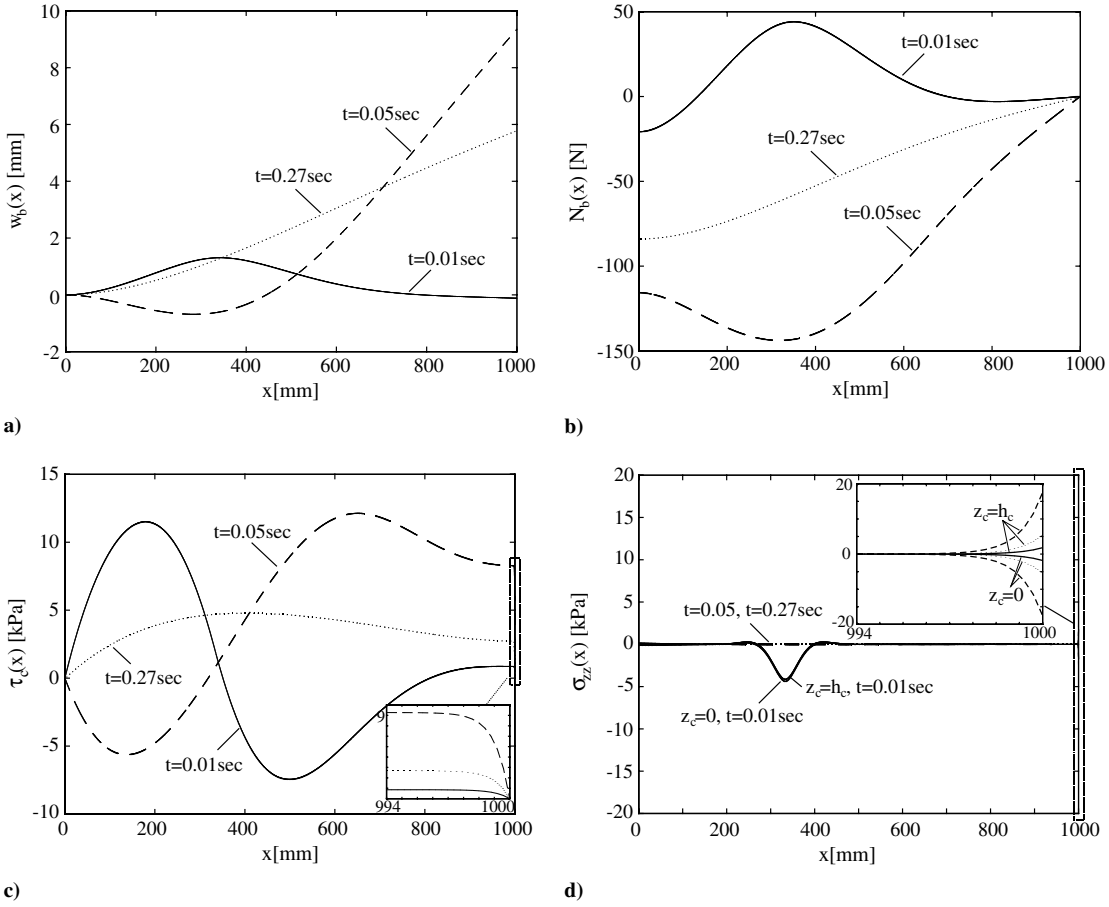

Fig. 15 Response of a cantilevered sandwich beam to an impulse load based on Kelvin–Voigt model for the core; distribution along the beam at $t = 0.01$, $t = 0.05$, and $t = 0.27$ s (solid line: $t = 0.01$ s; dashed line: $t = 0.05$ s; dotted line: $t = 0.27$ s): a) transverse deflection of the lower face sheet, b) axial force in the lower face sheet, c) transverse shear stresses in the core, d) transverse normal stresses at the core interfaces.

4.5 Hz, which corresponds to the first mode of flexural vibration. This value is in reasonable agreement with the experimental results. The second frequency equals about 18.8 Hz and corresponds to the second mode of flexural vibration. The different types of responses outlined in Figs. 12 and 13 highlight the differences between the two fundamental viscoelastic models and point in favor of using them as building blocks for refined viscoelastic models.

The time variation of the transverse (vertical) acceleration of the lower aluminum face sheet under the impulse load is studied in Fig. 14. The response is compared with the experimental results of Barbosa and Farage [40]. Figure 14a shows that the results of the Kelvin–Voigt model are in fair agreement with the experimental ones. The discrepancies at some points are due to the approximated impulse model that was adopted for the theoretical computation, due to the uncertainties with regard to the magnitude and duration of the applied load, and due to the use of a single retardation time in the viscoelastic Kelvin–Voigt model, which is not enough to represent a real viscoelastic material. On the other hand, excluding the first cycle, the prediction of Maxwell's model is far from the experimental results (Fig. 14b). These differences highlight the role of the detailed viscoelastic characteristics of the core and the selection of the corresponding model.

Figure 15 shows the distribution of the transverse deflection, the axial force in the lower face sheet, and the interfacial stresses at three times, which correspond to the response at peak loading ($t = 0.01$ s), at the adjacent peak after the load is released ($t = 0.05$ s), and at the peak steady-state response ($t = 0.27$ s). For clarity, only the results that were obtained by the Kelvin–Voigt model, which is in better agreement with the experiments, are presented. Figure 15a shows that the deformation pattern of the lower face sheet at $t = 0.01$ s is similar to the classical second mode of flexural vibration of a cantilevered beam. On the other hand, as the load is released, the second mode of vibration is damped, as shown by the response at $t = 0.05$ s. After 0.27 s, the deformation pattern becomes similar to the first mode of vibration and the second mode is completely damped (see also Fig. 12).

Figures 15b–15d show the variation of the distribution of the internal forces and stresses with time. Because of the nature of the concentrated impulse loading, it is seen that, at $t = 0.01$ s, the load induces concentrated forces and stresses (local response) at its close vicinity ($x = L/3$). This localized response propagates through the length of the beam and reaches an almost steady state at $t = 0.05$ s where the entire structure is affected by the loading. Figure 15d shows that localized transverse normal stresses develop in the core near the location of the load at $t = 0.01$ s. At $t = 0.05$ s and 0.27 s, these stress concentrations vanish, and the stresses at the free edge of the beam ($x = L$) are amplified. These results demonstrate the importance of the localized effects in the viscoelastic dynamic response of the sandwich beam, and reveal the capabilities of the proposed model.

VI. Conclusions

A theoretical model for the dynamic analysis of sandwich beams with soft viscoelastic cores has been developed. Along with the viscoelastic characteristics, the formulation has taken into account the shear deformability and the transverse (through the height) compressibility of the core under the framework of a high-order theory. The local effects (stress concentrations) and interfacial stresses that characterize sandwich structures, their variation in time, and the transient damped response of the viscoelastic sandwich beam have also been considered.

The formulation has introduced the viscoelastic characteristics of the core through the basic Kelvin–Voigt and Maxwell models with a single retardation/relaxation time. The governing equations of the two structural models and the corresponding numerical tools for the

solution in the time domain have been derived. These two models have provided the basic tools for the analysis of soft core sandwich beams with different types of viscoelastic cores as well as the theoretical and mathematical basis for the construction of more complex and more refined viscoelastic models. This has been demonstrated through an analytical formulation of a generalized Maxwell model and a standard linear solid viscoelastic model.

The numerical results have examined the response of sandwich beams with different types of viscoelastic cores and have been compared with experimental results available in the literature. The numerical study has quantified the damping characteristics introduced due to the viscoelastic core and its impact on the global and localized response of the beam. It has also revealed the different physical aspects described by the Kelvin–Voigt and Maxwell models, highlighted their characteristics, and opened the way for their potential augmentation to more advanced viscoelastic theories, including ones with multiple retardation/relaxation times. Although the proposed model is applicable for restricted frequency range, as the frequency and temperature dependence of the material constants have not been considered, the paper reveals and highlights some aspects of the dynamic behavior of modern sandwich beams with soft viscoelastic cores, and provides a basic theoretical modeling approach for more refined theoretical models to be developed.

References

[1] Lifshitz, J. M., and Liebowitz, M., "Optimal Sandwich Beam Design for Maximum Viscoelastic Damping," *International Journal of Solids and Structures*, Vol. 23, No. 7, 1987, pp. 1027–1034. doi:10.1016/0020-7683(87)90094-1

[2] Moreira, R. A. S., Dias Rodrigues, J., and Ferreira, A. J. M., "A Generalized Layerwise Finite Element for Multi-Layer Damping Treatments," *Computational Mechanics*, Vol. 37, No. 5, 2006, pp. 426–444. doi:10.1007/s00466-005-0714-1

[3] Wang, G., and Wereley, N. M., "Spectral Finite Element Analysis of Sandwich Beams with Passive Constrained Layer Damping," *Journal of Vibration and Acoustics*, Vol. 124, No. 3, 2002, pp. 376–386. doi:10.1115/1.1469007

[4] Daya, E. M., and Potier-Ferry, M., "A Numerical Method for Nonlinear Eigenvalue Problems Application to Vibrations of Viscoelastic Structures," *Computers and Structures*, Vol. 79, No. 5, 2001, pp. 533–541. doi:10.1016/S0045-7949(00)00151-6

[5] Dwivedy, S. K., Sahu, K. C., and Babu, S. K., "Parametric Instability Regions of Three-Layered Soft-Cored Sandwich Beam Using Higher-Order Theory," *Journal of Sound and Vibration*, Vol. 304, Nos. 1–2, 2007, pp. 326–344. doi:10.1016/j.jsv.2007.03.016

[6] Frostig, Y., and Baruch, M., "Free Vibrations of Sandwich Beams with a Transversely Flexible Core: A High Order Approach," *Journal of Sound and Vibration*, Vol. 176, No. 2, 1994, pp. 195–208. doi:10.1006/jsvi.1994.1368

[7] Sisemore, C. L., and Darvennes, C. M., "Transverse Vibration of Elastic-Viscoelastic-Elastic Sandwich Beams. Compression: Experimental and Analytical Study," *Journal of Sound and Vibration*, Vol. 252, No. 1, 2002, pp. 155–167. doi:10.1006/jsvi.2001.4038

[8] Fujii, T., "Dynamic Response of Sandwich Beams with an Adhesive Damping Layer (Generalized Maxwell Model for a Viscoelastic Adhesive Layer)," *International Journal of Adhesion and Adhesives*, Vol. 13, No. 3, 1993, pp. 201–209. doi:10.1016/0143-7496(93)90043-9

[9] Berthelot, J. M., Assarar, M., Sefrani, Y., and El Mahi, A., "Damping Analysis of Composite Materials and Structures," *Composite Structures*, Vol. 85, No. 3, 2008, pp. 189–204. doi:10.1016/j.compstruct.2007.10.024

[10] Park, J., "Transfer Function Methods to Measure Dynamic Mechanical Properties of Complex Structures," *Journal of Sound and Vibration*, Vol. 288, Nos. 1–2, 2005, pp. 57–79. doi:10.1016/j.jsv.2004.12.019

[11] Mead, D. J., and Markus, S., "The Forced Vibration of Three-Layer, Damped Sandwich Beam with Arbitrary Boundary Conditions," *Journal of Sound and Vibration*, Vol. 10, No. 2, 1969, pp. 163–175. doi:10.1016/0022-460X(69)90193-X

[12] Rao, D. K., "Frequency and Loss Factor of Sandwich Beams Under Various Boundary Conditions," *Journal of Mechanical Engineering Science*, Vol. 20, No. 5, 1978, pp. 271–282. doi:10.1243/JMES_JOUR_1978_020_047_02

[13] Lee, H. H., "Non-Linear Vibration of Multilayer Sandwich Beams with Viscoelastic Layers," *Journal of Sound and Vibration*, Vol. 216, No. 4, 1998, pp. 601–621. doi:10.1006/jsvi.1998.1716

[14] Kerwin, E. M., Jr., "Damping of Flexural Waves by Constrained Viscoelastic Layer," *Journal of the Acoustical Society of America*, Vol. 31, No. 7, 1959, pp. 952–962. doi:10.1121/1.1907821

[15] DiTaranto, R. A., "Theory of Vibratory Bending for Elastic and Viscoelastic Layered Finite-Length Beams," *Journal of Applied Mechanics*, Vol. 32, No. 4, 1965, pp. 881–886.

[16] Galucio, A. C., Deü, J. F., and Ohayon, R., "Finite Element Formulation of Viscoelastic Sandwich Beams Using Fractional Derivative Operators," *Computational Mechanics*, Vol. 33, No. 4, 2004, pp. 282–291. doi:10.1007/s00466-003-0529-x

[17] Sakiyama, T., Matsuda, H., and Morita, C., "Free Vibration Analysis of Sandwich Beam with Elastic or Viscoelastic Core by Applying the Discrete Green Function," *Journal of Sound and Vibration*, Vol. 191, No. 2, 1996, pp. 189–206. doi:10.1006/jsvi.1996.0115

[18] Meunier, M., and Shenoi, R. A., "Forced Response of FRP Sandwich Panels with Viscoelastic Materials," *Journal of Sound and Vibration*, Vol. 263, No. 1, 2003, pp. 131–151. doi:10.1016/S0022-460X(02)01101-X

[19] Hunston, D., Miyagi, Z., Schultheisz, C., and Zaghi, S., "The Sandwich Bending Specimen for Characterizing Adhesive Properties," *Mechanics of Time-Dependent Materials*, Vol. 7, No. 1, 2003, pp. 71–88. doi:10.1023/A:1024091302445

[20] Pradeep, V., Ganesan, N., and Bhaskar, K., "Vibration and Thermal Buckling of Composite Sandwich Beams with Viscoelastic Core," *Composite Structures*, Vol. 81, No. 1, 2007, pp. 60–69. doi:10.1016/j.compstruct.2006.05.011

[21] Nayfeh, S. A., "Damping of Flexural Vibration in the Plane of Lamination of Elastic-Viscoelastic Sandwich Beams," *Journal of Sound and Vibration*, Vol. 276, Nos. 3–5, 2004, pp. 689–711. doi:10.1016/j.jsv.2003.08.034

[22] Frostig, Y., Baruch, M., Vilnai, O., and Sheinman, I., "High-Order Theory for Sandwich-Beam Bending with Transversely Flexible Core," *Journal of Engineering Mechanics*, Vol. 118, No. 5, 1992, pp. 1026–1043. doi:10.1061/(ASCE)0733-9399(1992)118:5(1026)

[23] Douglas, B. E., and Yang, J. C. S., "Transverse Compressional Damping in the Vibratory Response of Elastic-Viscoelastic-Elastic Beams," *AIAA Journal*, Vol. 16, No. 9, 1978, pp. 925–930. doi:10.2514/3.7595

[24] Hao, M., and Rao, M. D., "Vibration and Damping Analysis of a Sandwich Beam Containing a Viscoelastic Constraining Layer," *Journal of Composite Materials*, Vol. 39, No. 18, 2005, pp. 1621–1643. doi:10.1177/0021998305051124

[25] Douglas, B. E., "Compressional Damping in Three-Layer Beams Incorporating Nearly Incompressible Viscoelastic Cores," *Journal of Sound and Vibration*, Vol. 104, No. 2, 1986, pp. 343–347. doi:10.1016/0022-460X(86)90273-7

[26] Bai, J. M., and Sun, C. T., "The Effect of Viscoelastic Adhesive Layers on Structural Damping of Sandwich Beams," *Mechanics of Structures and Machines*, Vol. 23, No. 1, 1995, pp. 1–16. doi:10.1080/08905459508905225

[27] Baber, T. T., Maddox, R. A., and Orozco, C. E., "A Finite Element Model for Harmonically Excited Viscoelastic Sandwich Beams," *Computers and Structures*, Vol. 66, No. 1, 1998, pp. 105–113. doi:10.1016/S0045-7949(97)00046-1

[28] Miles, R. N., and Reinhall, P. G., "An Analytical Model for the Vibration of Laminated Beams Including the Effects of Both Shear and Thickness Deformation in the Adhesive Layer," *Journal of Vibration Acoustics Stress and Reliability in Design*, Vol. 108, No. 1, 1986, pp. 56–64.

[29] Frostig, Y., and Thomsen, O. T., "High-Order Free Vibration of Sandwich Panels with a Flexible Core," *International Journal of Solids and Structures*, Vol. 41, Nos. 5–6, 2004, pp. 1697–1724. doi:10.1016/j.ijsolstr.2003.09.051

[30] Schwarts-Givli, H., Rabinovitch, O., and Frostig, Y., "High Order Nonlinear Contact Effects in Cyclic Loading of Delaminated Sandwich Panels," *Composites, Part B: Engineering*, Vol. 38, No. 1, 2007, pp. 86–101.

doi:10.1016/j.compositesb.2006.03.011
[31] Schwarts-Givli, H., Rabinovitch, O., and Frostig, Y., "High Order Nonlinear Contact Effects in the Dynamic Behavior of Delaminated Sandwich Panels with Flexible Core," *International Journal of Solids and Structures*, Vol. 44, No. 1, 2007, pp. 77–99. doi:10.1016/j.ijsolstr.2006.04.016
[32] Schwarts-Givli, H., Rabinovitch, O., and Frostig, Y., "Free Vibrations of Delaminated Unidirectional Sandwich Panels with a Transversely Flexible Core: A Modified Galerkin Approach," *Journal of Sound and Vibration*, Vol. 301, Nos. 1–2, 2007, pp. 253–277. doi:10.1016/j.jsv.2006.10.006
[33] Hamed, E., and Rabinovitch, O., "Damping and Viscoelastic Dynamic Response of RC Flexural Members Strengthened with Adhesively Bonded Composite Materials," *Journal of Engineering Mechanics*, Vol. 133, No. 12, 2007, pp. 1278–1289. doi:10.1061/(ASCE)0733-9399(2007)133:12(1278)
[34] Ferry, J. D., *Viscoelastic Properties of Polymers*, Wiley, New York, 1970.
[35] Hamed, E., and Rabinovitch, O., "Viscoelastic Behavior of Soft Core Sandwich Panels Under Dynamic Loading," edited by A. J. M. Ferreira, Faculty of Engineering, Univ. of Porto, Porto, Portugal, 2008, pp. 1109–1120.
[36] Wunderlich, W., and Pilkey, W. D., *Mechanics of Structures: Variational and Computational Methods*, 2nd ed., CRC Press, Boca Raton, FL, 2003.
[37] Sokolinsky, V. S., and Nutt, S. R., "Consistent Higher-Order Dynamic Equations for Soft-Core Sandwich Beams," *AIAA Journal*, Vol. 42, No. 2, 2004, pp. 374–382. doi:10.2514/1.2742
[38] Newmark, N. M., "A Method of Computation of Structural Dynamics," *Journal of the Engineering Mechanics Division, American Society of Civil Engineers*, Vol. 85, No. EM3, 1959, pp. 67–94.
[39] Stoer, J., and Bulirsch, R., *Introduction to Numerical Analysis*, Springer, New York, 1993.
[40] Barbosa, F. S., and Farage, M. C. R., "A Finite Element Model for Sandwich Viscoelastic Beams: Experimental and Numerical Assessment," *Journal of Sound and Vibration*, Vol. 317, Nos. 1–2, 2008, pp. 91–111. doi:10.1016/j.jsv.2008.03.013
[41] Adams, R., Maheri, R., and Hugon, J., "The Vibration Properties of Sandwich Panels: Eigenfrequencies and Damping," edited by A. J. M. Ferreira, Faculty of Engineering, Univ. of Porto, Porto, Portugal, 2008, pp. 908–918.

R. Kapania
Associate Editor